ARTICLE IN PRESS

Engineering xxx (xxxx) xxx

Contents lists available at ScienceDirect

Engineering

journal homepage: www.elsevier.com/locate/eng

Research
Textile Engineering—Review

3D Printing Strategies for Precise and Functional Assembly of Silk-based Biomaterials

Xiaoliang Cui [a], Jun Zhang [a,*], Yan Qian [a], Siqi Chang [a], Benjamin J. Allardyce [b], Rangam Rajkhowa [b], Hui Wang [a,*], Ke-Qin Zhang [a,*]

[a] National Engineering Laboratory for Modern Silk, College of Textile and Clothing Engineering, Soochow University, Suzhou 215123, China
[b] Institute for Frontier Materials, Deakin University, Geelong, VIC 3216, Australia

ARTICLE INFO

Article history:
Available online xxxx

Keywords:
3D printing
Bioink
Bioprinting
Silk fibroin

ABSTRACT

In recent years, significant progress has been made in both three-dimensional (3D) printing technologies and the exploration of silk as an ink to produce biocompatible constructs. Combined with the unlimited design potential of 3D printing, silk can be processed into a broad range of functional materials and devices for various biomedical applications. The ability of silk to be processed into various materials, including solutions, hydrogels, particles, microspheres, and fibers, makes it an excellent candidate for adaptation to different 3D printing techniques. This review presents a didactic overview of the 3D printing of silk-based materials, major categories of printing techniques, and their prototyping mechanisms and structural features. In addition, we provide a roadmap for researchers aiming to incorporate silk printing into their own work by summarizing promising strategies from both technical and material aspects, to relate state-of-the-art silk-based material processing with fast-developing 3D printing technologies. Thus, our focus is on elucidating the techniques and strategies that advance the development of precise assembly strategies for silk-based materials. Precise printing (including high printing resolution, complex structure realization, and printing fidelity) is a prerequisite for the digital design capability of 3D printing technology and would definitely broaden the application era of silk, such as complex biomimetic tissue structures, vasculatures, and transdermal microneedles.

1. Introduction

Three-dimensional (3D) printing technology, also known as additive manufacturing (AM), is defined as "the process of joining materials to make objects from 3D model data, frequently layer-by-layer, as opposed to subtractive manufacturing methods" [1]. In recent years, 3D printing has developed rapidly, with applications ranging from automotive materials to organ transplantation [2–5]. Artificial tissues and organs created using 3D printing have the potential to address the challenges in tissue repair and organ transplantation [6,7]. Considering this significance, considerable research effort has been made to improve the methods (printing techniques) and materials (printing inks) used to create biomimetic materials for tissue engineering.

The major advantage of 3D printing is the direct realization of customized designs, particularly those with sophisticated geometries and internal structures, which is not possible using traditional fabrication strategies. However, despite significant advances in printing methods, material development has limited the potential for 3D printing and remains a bottleneck in the field. Over the last decade, deliberate attempts have been made to expand the toolkit of materials for 3D printing applications to meet the potential of 3D printing technologies. An ideal printing ink should exhibit good printability, printing accuracy, and mechanical integrity. For biomedical applications, the ink also requires biocompatibility to provide a cell-friendly environment, particularly for cell-encapsulating bioprinting [8]. However, developing a material that satisfies all these requirements remains a key challenge. For example, an ink with excellent printing fidelity and robust mechanical properties may be too stiff to support live-cell printing or enable post-printing cell proliferation.

In this review, we focus on the use of silk for 3D printing. Silk has been extensively utilized as a biomaterial in Food and Drug

* Correspondence authors.
E-mail addresses: junzhang@suda.edu.cn (J. Zhang), whui@suda.edu.cn (H. Wang), kqzhang@suda.edu.cn (K.-Q. Zhang).

https://doi.org/10.1016/j.eng.2023.09.022
2095-8099/

Please cite this article as: X. Cui, J. Zhang, Y. Qian et al., 3D Printing Strategies for Precise and Functional Assembly of Silk-based Biomaterials, Engineering, https://doi.org/10.1016/j.eng.2023.09.022

Administration-approved sutures for surgical operations. Among the different types of silk, that derived from the domestic silkworm *Bombyx mori* is the most thoroughly characterized and widely used for biomaterial applications [9]. The abundance of silkworm silk makes it an excellent candidate for the development of biomedical devices. Silk fibroin (SF), a structural protein that remains after degumming, is an attractive material for tissue engineering owing to its unique combination of elasticity, strength, and good mammalian cell compatibility [10]. SF can be chemically modified to incorporate features such as cell–recognition motifs, minerals, or cellular growth factors. It has been observed to be biocompatible both *in vitro* [11–14], supporting a range of primary cells and cell lines, and *in vivo* [15–17]. Silk has demonstrated promise for tissue engineering in applications such as bone [12,18], cartilage [19,20], tendon, and ligament repair [17,21,22]. These unique characteristics make it an ideal biomaterial for 3D printing of bio-scaffolds.

Herein, we systematically review the printing mechanism, material processing, printing requirements, and structural characteristics of SF-based 3D printing (Fig. 1). We also discuss the most suitable applications for different printing techniques and printed structures. In addition, we propose promising strategies for further improvement of the printing quality, for instance resolution, fidelity, functionality, to broaden the application of SF-based 3D printed materials in different fields.

2. 3D printing overview

According to the ISO/ASTM 52900 standard [23], 3D printing techniques can be classified into seven major categories: material extrusion (ME), powder bed fusion (PBF), binder jetting (BJ), vat polymerization (VP), direct energy deposition (DED), material jetting (MJ), and sheet lamination (SL) [24], with different material formats suitable for individual printing techniques. A schematic of the different printing processes is shown in Fig. 2. Based on different prototyping mechanisms and feedstock material formats, these seven techniques can be grouped into four major systems: extrusion, powder, photopolymerization, and solid bulk. Extrusion printing primarily involves ME, which relies on ME through a nozzle (Fig. 2(a)). Two main printing techniques fall into this category: fused filament fabrication (FFF) and direct ink writing (DIW). Powder system include PBF, BJ, and DED. PBF and BJ print objects by spreading powder layers on a powder bed; the only difference is that PBF uses a laser source to fuse particles, whereas BJ applies a liquid binder to bind the particles together (Fig. 2(b)). In contrast, DED deposits the powder material on a substrate through a nozzle and then fuses the particles with a laser source (Fig. 2(d)). The photopolymerization system primarily includes VP and MJ, as shown in Figs. 2(c) and (e). The printing mechanism of both techniques relies on ultraviolet (UV) or light-induced photopolymerization of the printing material, except that the printed object is printed and lifted from a photopolymer vat in VP, whereas MJ uses a printhead to jet the photopolymer onto the build platform to form the part. The last group, the solid bulk system, primarily includes SL, in which objects are formed by bonding materials in a sheet format (Fig. 2(f)).

From the perspective of printing materials, different 3D printing techniques can be further categorized into four types based on the dimensions of the building unit: dot, line, surface, and volume. An overview of the printing speed and resolution of the various printing techniques is shown in Fig. 3. With increasing building unit dimensions (from dot to volume), the printing speed typically increases at the cost of decreased resolution, except for digital light processing (DLP) and continuous liquid interface production (CLIP), both of which are VP techniques. Generally, the printing resolution is in the order of photopolymerization > powder > extrusion > solid bulk system, whereas the printing speed varies based on the specific printing technique.

Regarding printing with silk-based materials or bioprinting, where living organisms such as cells are printed together with aqueous biomaterials, techniques with harsh processing conditions, such as lasers, are unsuitable (PBF, DED, and SL). The mainstream printing technologies for prototyping silk include ME, VP, and MJ, which are marked with solid stars in Fig. 3, and they are the focus of discussion in the following sections. With the highest printing resolution, VP is the most rapidly developing printing technology. The recently emerging VP techniques suitable for printing SF have not yet been explored and are marked with a hollow star in the figure; they are explored in detail in Section 7.1. Additionally, note that some attempts have been made to use silk powder directly as the powder matrix in BJ printing technology [25], as marked with a smiling face in Fig. 3.

As the most crucial component of 3D printing, inks determine the structure and function of the tissue formed by providing a steady and biocompatible microenvironment for cell proliferation and differentiation. For biomedical applications, an ideal bioink requires excellent biocompatibility to keep cells active and functional, good printability to form scaffolds by 3D printing, suitable mechanical strength to maintain the 3D printed structure, and biodegradation during transplantation. However, traditional inks, including alginate and synthetic polymer materials, cannot be used owing to various problems, such as the difficulty in degrading alginate and the weak mechanical strength of polyethylene glycol (PEG). Silk has demonstrated remarkable development potential owing to its excellent biocompatibility, biodegradability, minor inflammatory reactions, and tunable mechanical properties when used as a solid material [26,27]. Additionally, because silk-based bioinks are naturally amphiphilic, they can be used to produce protein drops in the pico- to nano-liter range by adjusting the ink rheology with different pH and ionic strength values. By dissolving degummed silk in a chaotropic solvent, such as lithium bromide, silk fibers can be converted to a liquid and re-solidified into a range of regenerated products, including powders, gels [28–30], sponges

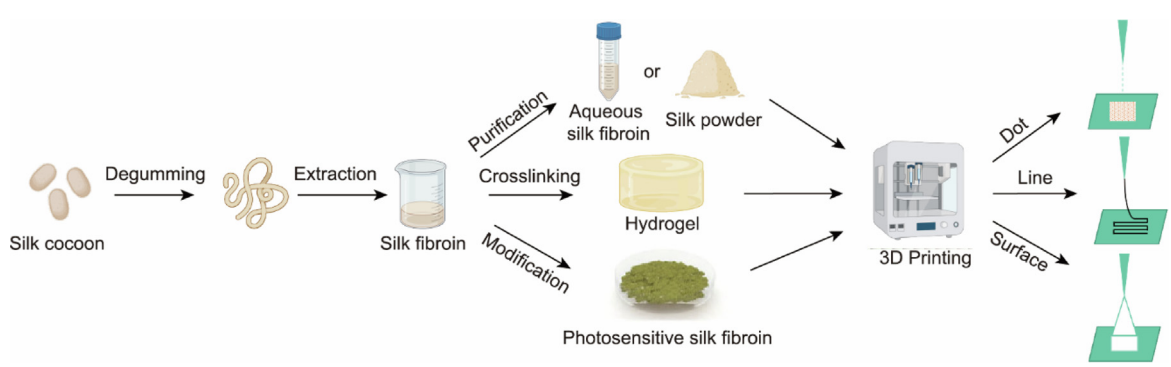

Fig. 1. Schematic of different types of 3D printing using silk as the bioink

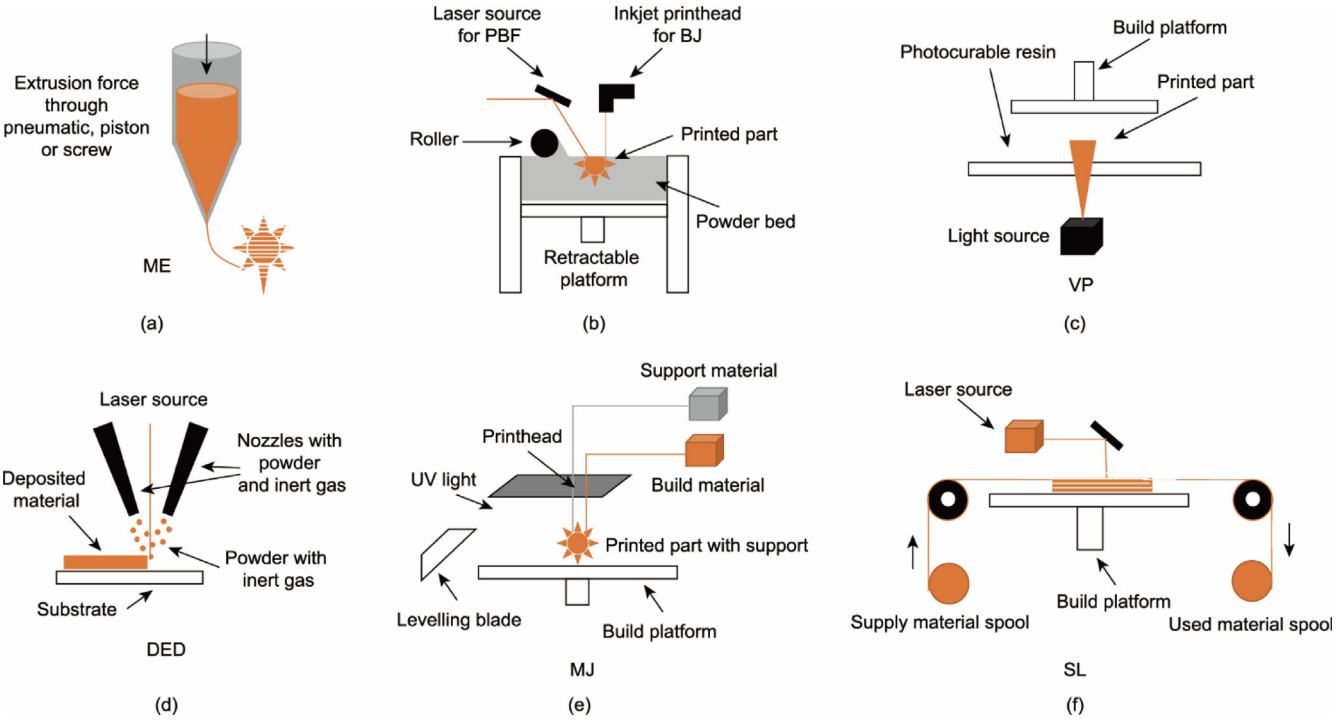

Fig. 2. Schematic of the printing process for typical 3D printing systems. (a) ME, (b) PBF and BJ, (c) VP, (d) DED, (e) MJ, and (f) SL

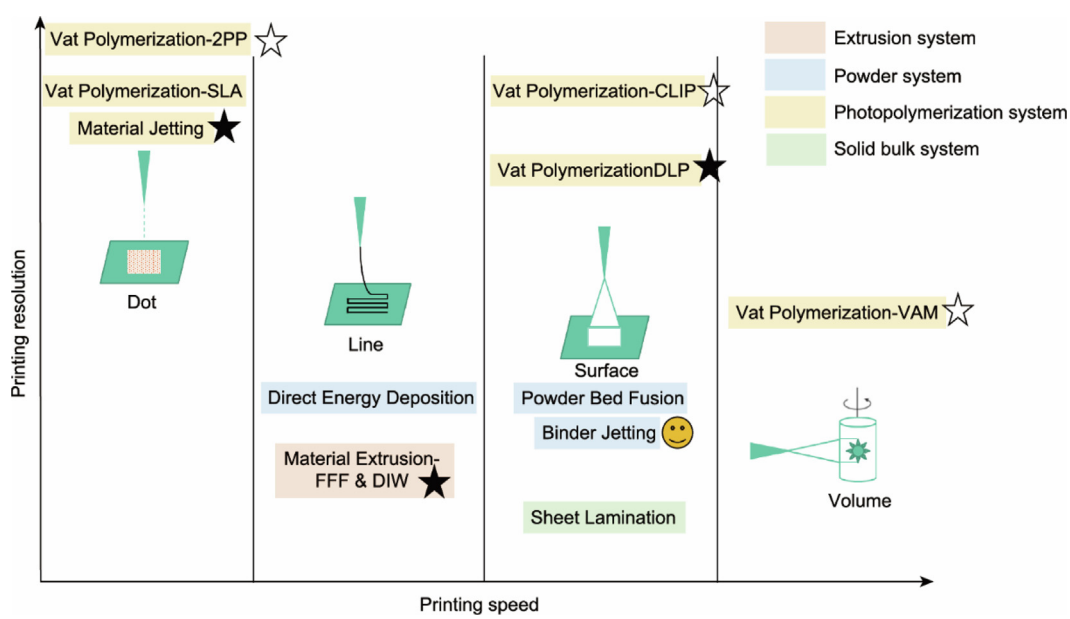

Fig. 3. Schematic of different 3D printing approaches

[31,32], and films [33–35], for biomedical applications. Owing to these unique characteristics, it has been considered as a suitable candidate for satisfying the requirements of different 3D printing methods.

3. Silk as printing ink

3.1. Silk structure

Natural silkworm silk is composed of SF, a structural filament, and sericin, a glue-like coating that binds to the cocoons. Sericin protein, which accounts for 19%–28% of the weight of silk cocoons, is predominantly hydrophilic and can be removed from fibroin by degumming, which most commonly involves boiling cocoons in an aqueous alkaline solution [9]. Degumming is critical for the use of silk in biomedical applications because it can inhibit fibroin processing, such as dissolution, and undegummed silk is associated with an immunogenic reaction in the body [36].

The structure of SF consists of a light chain (26 kilodaltons (kDa)) and a heavy chain (391 kDa) bound together by a disulfide bond between the cysteine-172 residue on the light chain and the cysteine-20 residue on the heavy chain [37,38]. A 25 kDa glycoprotein called P25, is also non-covalently linked to these chains, which facilitates this binding. The light chain, heavy chain, and P25 occur at a ratio of 6:6:1 in the natural fiber. The heavy chain is organized

into 12 repetitive crystalline domains and 11 amorphous domains [39]. It consists of a high proportion of repeats of a glycine-X dipeptide motif, where X is alanine in 64% of the repeats, serine in 22%, tyrosine in 10%, valine in 3%, and threonine in 1.3% [40]. Highly ordered hydrogen bonding within the hydrophobic domains form into anti-parallel β-sheets, which in turn pack into dense β-sheet nanocrystals with reported dimensions of between 2.6 nm × 3.2 nm × 11.5 nm and 21 nm × 6 nm × 2 nm [40,41]. In contrast, light chains are relatively elastic and hydrophilic blocks [10,42].

Beyond the secondary structure, SF can form different tertiary and quaternary forms, the most common of which are silk I, silk II, and silk III [37]. Silk I refers to the random coil and α-helix arrangements, which are random weak interactions between amino acids with bulky and polar side chains, also known as the amorphous region. In this conformation, the repetitive β-sheet forming domains of SF do not interact strongly. Silk II is silk when it has self-assembled to form highly crystalline anti-parallel β-sheet nanocrystals or fragments embedded as physical crosslinks within amorphous domains. Silk III is observed at the air–water interface and exhibits a three-fold helical structure [43]. With its unique protein sequence, SF can undergo complex intra- and inter-molecular self-assembly [9]. As a result, the secondary structure of the protein and orientation of the crystalline domains are strongly influenced by the environment and processing conditions. For example, silk I tends to transition into silk II owing to elevated temperature, the presence of dehydrating solvents, and shearing forces [36]. These structural characteristics endow SF with various qualities, making it an excellent biomaterial.

3.2. Silk printing ink formats

Among the different silk formats, attempts have been made to use silk particles, micro/nano fibers, and solutions in the 3D printing of bio-scaffolds, as summarized in Table 1. As reinforcing and functional parts, native silk particles and micro/nanofibers processed from physical milling and chemical etching have been used in composite scaffold printing with a matrix material such as chitosan [44,45], xanthan gum [46], and polycaprolactone (PCL) [47]. The majority of studies on SF printing use a regenerated silk solution as the printing ink with different methods to assist with prototyping, such as gelation by inducing SF secondary structure changes, chemical modification, photopolymerization, and hybrid printing. The detailed printing strategies and mechanisms are thoroughly summarized according to the different features of the three mainstream printing techniques. Promising gelation and chemical modification methods have also been proposed as novel prototyping methods (Section 7.2). In the following sections, we introduce the printing mechanism, ink requirements, and silk-based ink processing using the abovementioned primary printing techniques and promising strategies that have not yet been explored.

4. Material jetting

4.1. Printing mechanism and ink requirements

MJ, also known as inkjet-based 3D printing, is often considered a facile, cost-effective, and eco-friendly method for AM [48,49]. Typically, ink droplets activated by piezoelectric or thermal forces are deposited onto a substrate from ink cartridges to form a pre-designed pattern (Fig. 4(a)) [50,51]. Printing ink frequently has a low viscosity to ensure good deposition from ultrafine nozzles [52]. Because of its precision in droplet volume down to picolitre [53,54] and layer-by-layer printing characteristics, MJ can print both two-dimensional (2D) patterns with high resolution and multifunctional 3D structures with good accuracy [50]. MJ printing with SF ink typically remains at the 2D level.

The Z number is commonly used to evaluate printability during MJ printing. The Z number, which is the inverse of the Ohnesorge number (Oh), is calculated using the formulas shown in Eqs. (1) and (2) [55]:

$$\mathrm{Oh} = \frac{\eta}{\sqrt{\rho\gamma a}} \tag{1}$$

$$Z = \frac{1}{\mathrm{Oh}} \tag{2}$$

where η is the viscosity of the ink, ρ is the ink density, γ is the surface tension, and a stands for the radius of the nozzle. Z is a dimensionless number used to predict the formation of stable droplets. Stable droplets typically form when $1 < Z < 10$ [54]. If $Z < 1$, the ink may block the nozzle owing to high viscous forces. However, when the Z number exceeds 10, unwanted satellite droplets may occur. Thus, droplet formation and stability depend on the dynamic regulation of ink viscosity, density, tension, and nozzle radius. Viscosity is related to the stability of the drop, and a high viscosity may cause the nozzle to clog.

A sufficient surface tension is also critical for MJ printing of silk inks at it holds the meniscus at the nozzle and prevents the tip from submerging; is it frequently set in the range of 0.04–0.07 $\mathrm{n{\cdot}L{\cdot}mol^{-1}}$ at room temperature [54]. The high surface tension would make the droplets fall faster. A high surface tension would cause the droplets to fall faster. Moreover, the resolution limit depends primarily on the nozzle size. The distance between the droplets must be adjusted based on the droplet size to generate a continuous line [50,56].

4.2. Silk-based MJ printing ink

Owing to its flexibility in terms of nozzle size, number, placement of droplets, and printing temperature, MJ is considered an effective method of controlling sol–gel reactions [56]. SF has been used as an excellent bio-ink for MJ printing because of its aqueous solubility, good biocompatibility, easily controllable crystal

Table 1
SF as printing ink

SF format	Processing method	Printing technology	Role
Particles	Milling	BJ	Printing powder matrix
	Milling	ME	Reinforcing filler
Micro/nano fiber	Chemical etching	ME	Reinforcing filler
Solution	Dissolving and regeneration	MJ	Printing ink
	Dissolving and regeneration	ME	Printing ink
	Dissolving, regeneration and chemical modification	VP	Printing ink

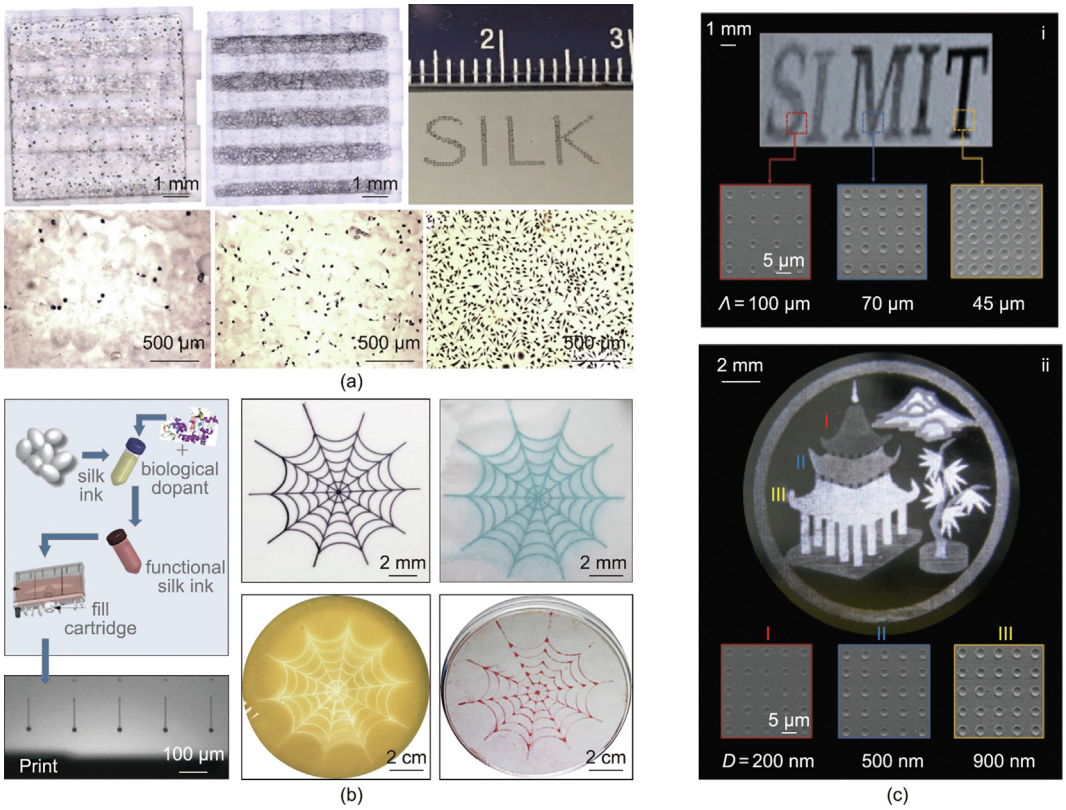

Fig. 4. (a) Biocompatible silk films with selectively printed methanol treated domains prepared by reactive inkjet printing. Reproduced from Ref. [52] with permission of Springer, ©2016. (b) Schematic of the preparation of functional silk inks and examples of patterned functional silk inks by inkjet printing. Reproduced from Ref. [54] with permission of Wiley, ©2015. (c) Optical and SEM images of microhole arrays with different periodicities (i) and depths (ii) generated on silk substrate by silk-based water lithography. *D*: the depth of the holes. Reproduced from Ref. [58] with permission of Wiley, ©2018.

Table 2
SF-based inkjet printing strategies

Classifier	Ink Composition	Crosslinking type	Prototyping mechanism	References
Pure SF	SF	Physical	Methanol treatment to convert the SF secondary structure from silk I into silk II.	[50-52,55-57,60]
Chemically modified SF	SF + HRP and H_2O_2	Chemical	Dityrosine bonds formation using HRP and H_2O_2 to partially crosslink SF and modulate ink viscosity for printing.	[63]
	SF + polylysine + polyglutamic acid	Chemical	Diazonium activation of abundant tyrosine side chains in SF molecules followed by chemical conjugation of polylysine or polyglutamic acid to produce SF-polylysine and SF-polyglutamic polymers.	[61,62]
SF Hybrid	SF + collagen	Physical	Temperature induced solidification.	[58]
	SF + alginate	Ionic	Gel formation by using alginate and calcium chloride ($CaCl_2$) followed by enzymatic crosslinking of SF using HRP.	[63]

structure and degradation, polymorphic features, and versatile functionalization. The SF-based MJ printing strategies are summarized in Table 2. The use of methanol to create β-sheet structures is the most common method [50–52,55–57]. For example, a single layer of SF ink can be printed, followed by methanol deposition to promote β-sheet formation and facilitate the printing reaction. The crystallinity and surface properties of SF can be tuned by changing the SF-to-methanol ratio [52,56,57]. Moreover, some functional components such as nanoparticles, enzymes, antibiotics, growth factors, and antibodies are frequently mixed with SF ink for printing to achieve specific functions [54,58]. Umar et al. [48] introduced gold nanoparticles (AuNPs) into SF/dye ink and observed that the lasing wavelength can be slightly tuned by adding AuNPs to manufacture biomaterial photonic chips intended for advanced sensing and diagnostic applications. In addition to being used as a printing ink, SF can also serve as a protein substrate in film format [49,58,59].

In 2006, Kaplan et al. [60] reported successful cell patterning for the first time using inkjet deposition in a 0.6% water-based silk solution. The study created cellular patterns with 111 ± 24 μm resolution and demonstrated successful cell function regulation with such a method. However, the toxicity of methanol may hinder the encapsulation and growth of cells, which can be solved using chemical modification [51]. Suntivich et al. [61,62] introduced a

method for grafting polylysine and polyglutamic groups onto SF molecules, creating cationic and anionic sites and forming stable bonds upon alternate deposition. The results showed that the prepared SF nests can encapsulate *Escherichia coli* (*E. coli*) cells and print them into structures in a customized manner [61]. Another method is adding horseradish peroxidase (HRP) and hydrogen peroxide (H_2O_2) into SF solutions to form covalent dityrosine bonds between tyrosine residues and partially crosslink SF to modulate the ink viscosity for printing [50]. Additionally, hybrid inks exist in which SF is mixed with other materials such as collagen and alginate. In addition, freeze-drying post-treatment is required in some printing cases to preserve the printed structures and avoid melting [50].

Fig. 4 shows that the representative SF printing structures with MJ have excellent details but frequently remain at the 2D level. Cheryl et al. [52] produced a biocompatible film through the alternate printing of an SF aqueous solution and methanol using reactive inkjet printing. The inkjet-printed SF films were biocompatible with fibroblast cellular adhesion and proliferation on the film surface. Another advantage of SF-based inks is that they can be prepared using a water-based process, thus providing a wide range of opportunities by combining SF inks with other macromolecules such as antibodies, carbohydrates, lipids, nucleic acids, and functional polymers. This provides valuable avenues for printed functional forms, such as the design of sensors and assays. Tao et al. [54] synthesized a functional SF ink by introducing several biological dopants (Fig. 4(b)). The mechanical and biochemical properties were tuned by changing the SF polymorphism and adding other functional components. They also regulated the printing parameters of SF water lithography, which enabled the creation of grayscale structures [58]. As shown in Fig. 4(c), the individual letters of the "SIMIT" pattern are composed of 2D dot arrays with different lattice constants (Λ = 100, 70, and 45 μm, respectively), which shows a difference in terms of the shades. Such control over the pattern geometry, periodicity, and function of the silk water lithography promises a convenient "print-to-pattern" platform for biophotonics.

5. Material extrusion

5.1. Printing mechanism and ink requirements

The ME category has to primary types of printing: FFF and DIW. FFF printers are perhaps the most widely used household 3D printers. They use thermoplastics as printing materials using a melt-extrusion printing methodology. Despite the reports of regenerated silk exhibiting thermoplasticity under specific heating and pressurization conditions, its use in printing systems remains challenging [64]. The high printing temperatures required for this method also pose a challenge for SF, which can degrade or oxidize at elevated temperatures. However, Vyas et al. [47] used pulverized silk particles as a filler material for the FFF printing of PCL composite scaffolds, and the results showed a favorable cellular response with the addition of silk, suggesting that silk could help tune the degradation rate of PCL.

DIW is another extrusion-based printing method that can be considered an analogue to FFF. It enables the use of a wide range of fluids, as long as they have suitable rheological properties or can be modified to have the correct properties. During the DIW printing process, the ink is extruded and solidified in a designated area, and an object is printed layer by layer composed of filaments. It was first developed at Sandia National Laboratories, USA, as a moldless fabrication technique in 1996 [65,66]. Because of the wide range of material options and ease of handling, most published silk-based printing uses this method. Elevated temperatures are not required. However, DIW printing depends on the rheological properties of the printing ink. The most fundamental and critical properties, the desired rheological properties of DIW ink include the following:

① Good flow of the ink to be extruded out of the micron-sized nozzles without causing any blockage.

② Shear-thinning is favored for most inks in DIW, which means that the ink demonstrates solid-like behavior (storage modulus (G′) > loss modulus (G″)) in the static form and transforms into fluid behavior (G″ > G′) under shearing. This behavior is also demonstrated by the decrease in viscosity with increasing shear rate.

③ Instant ink solidification after extrusion is essential to ensure printing fidelity. This liquid-to-solid transition process can either rely on the suitable self-recovery properties of the ink to retain its storage modulus (G′) when deposited or can be induced by external sources, such as a coagulation bath (e.g., in alcohol to induce physical crosslinking) or UV (e.g., it requires the use of methacrylated silk).

In a typical flow process, the shear rate of a Newtonian fluid can be calculated according to the Mooney analysis [67]:

$$\dot{\gamma}_N = \frac{4Q}{\pi r^3} \tag{3}$$

where $\dot{\gamma}_N$ is the shear rate of the Newtonian fluid, Q is the volumetric flow rate ($mm^3 \cdot s^{-1}$), and r is the radius of the nozzle (mm). For non-Newtonian fluids, according to the power–law model [68], the equation can be corrected as

$$\dot{\gamma} = \frac{3n+1}{4n}\dot{\gamma}_N \tag{4}$$

where $\dot{\gamma}$ is the shear rate of the non-Newtonian fluid, and n is the flow index (non-Newtonian index). When n = 1, the fluid is Newtonian, when n > 1, the fluid exhibits shear thickening (dilatant), and when n < 1, the fluid exhibits shear thinning (pseudoplastic).

The pseudoplastic behavior of printing inks are expressed by the Herschel–Bulkley model:

$$\tau = \tau_\gamma + K\dot{\gamma}^n \tag{5}$$

where τ is the shear stress, τ_γ is the yield stress, K is the consistency, and n is the flow index [69]. Thus, the shear stress applied at the nozzle should exceed the yield stress of the ink to induce an ink flow. The correlation between ink rheology and printing prerequisites enables researchers to develop different types of silk-based DIW printing inks for various applications, as summarized in Fig. 5.

The shear rate–viscosity curve is often used to evaluate the flow properties of DIW printing ink. The apparent viscosity typically has been reported to be between 10^{-1} and 10^3 Pa·s at a shear rate of 0.1 s^{-1} to ensure proper printability [70]. In Figs. 5(a)–(d), all silk-based printing inks exhibit shear-thinning behavior, with the viscosity values falling within the printable range. Xuan et al. [71] observed that a pure SF solution exhibited an exponential increase in viscosity with increasing concentration, primarily because of increasing molecular entanglements. The SF inks were characterized to reveal concentration-dependent molecular mechanisms, such as tyrosine interactions, which may facilitate the sol-gel transition of SF. The hybrid printing ink composed of SF and alginate also exhibited evident shear-thinning behavior (Fig. 5(b)). The ink viscosity increased for DIW printing through the ionic crosslinking treatment of alginate [72]. A "CareGum" multifunctional ink composed of SF, tannic acid (TA), $CaCl_2$, and reduced graphene oxide (rGO) had a viscosity of 200–2000 Pa·s at a shear rate of 100 s^{-1} (Fig. 5(c)), which equaled the shear rate upon manual extrusion through a 22 gauge needle, providing guidance in the actual printing processing [73]. The viscosity of the SF ink could be tailored by introducing nano-fillers (Fig. 5(d)). An increase in

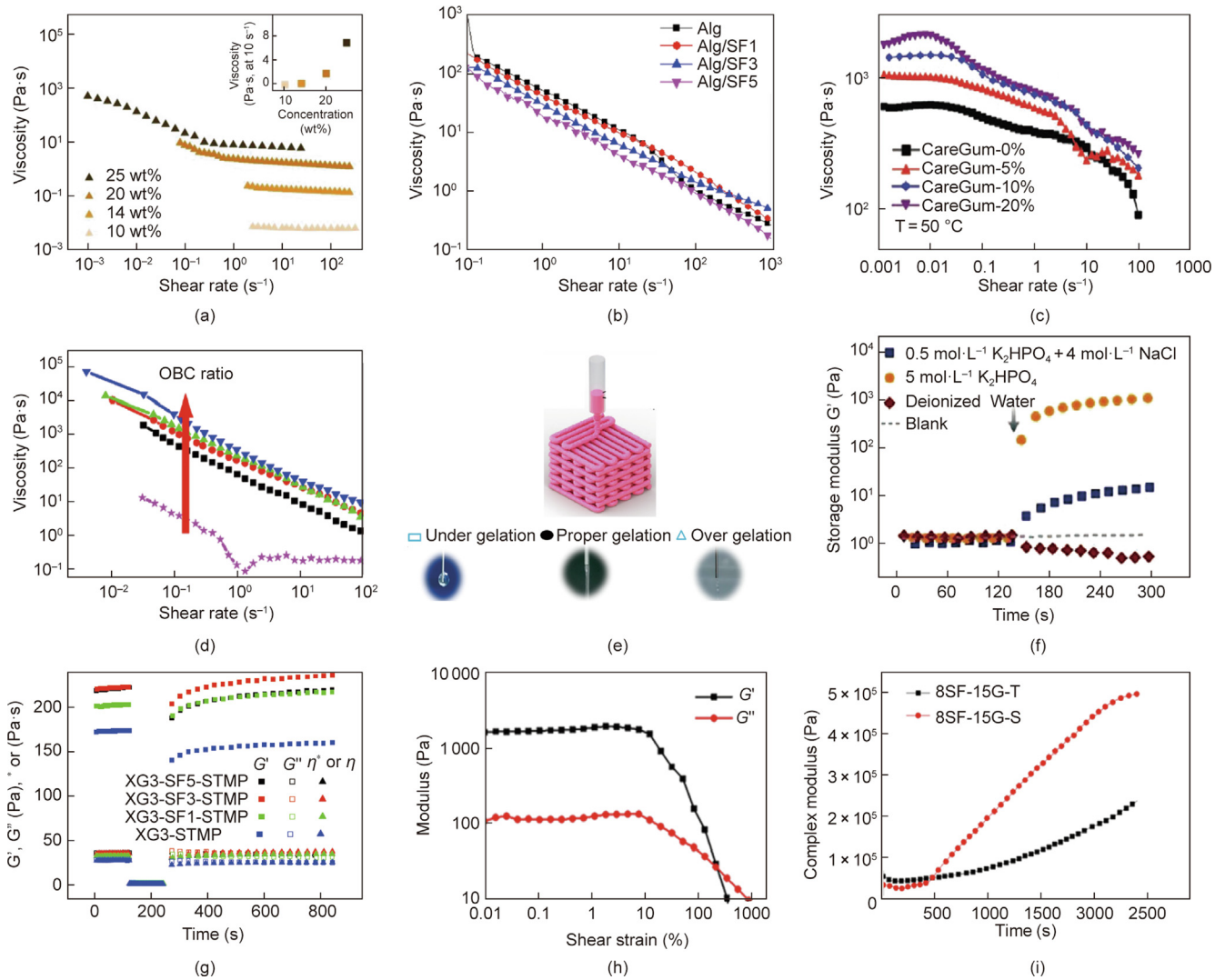

Fig. 5. (a) Shear rate–viscosity profiles of SF solution at 10, 14, 20, and 25 wt%. Inset shows the exponential increase of ink viscosity at 10 s^{-1} shear rate with increasing concentration. Reproduced from Ref. [71] with permission of MDPI, ©2022. (b) Shear-thinning behaviors of pre-crosslinked alginate (Alg) and alginate/SF solutions. Reproduced from Ref. [72] with permission of American Chemical Society, ©2021. (c) Shear rate–viscosity of different concentration of CareGum ink composed of SF, TA, $CaCl_2$, and rGO. Reproduced from Ref. [73] with permission of Wiley, ©2021. (d) Shear rate–viscosity of SF composite printing ink with different ratio of OBC nanofibrils. Reproduced from Ref. [74] with permission of Springer, ©2021. (e) Schematic of the extrusion printing process. The images of under, proper and over gelation are obtained from Ref. [75]. Reproduced from Ref. [75] with permission of KeAi, ©2022. (f) Oscillatory time sweep of SF ink with their storage modulus rising upon addition of different potassium concentrations. Reproduced from Ref. [76] with permission of Wiley, ©2020. (g) Oscillation time seep test of a printing ink composed of xanthan gum (XG) and SF. STMP: sodium trimetaphosphate, η: shear viscosity. Reproduced from Ref. [46] with permission of Elsevier, ©2020. (h) Amplitude sweep of a self-gelling ink composed of SF blends and gelatin (G). T: tyrosinase, S: sonication. Reproduced from Ref. [77] with permission of American Chemical Society, ©2019. (i) Gelation kinetics of SF ink with different crosslinking methods. Reproduced from Ref. [78] with permission of Elsevier, ©2015.

viscosity of approximately five-fold was observed with the addition of oxidized bacterial cellulose (OBC) nanofibrils to pure SF printing ink [74]. The ink rheology directly affects ink gelation upon extrusion and is thus detrimental to a successful extrusion printing process (Fig. 5(e)) [75].

Oscillation tests are commonly used in extrusion ink rheology measurements. As shown in Fig. 5(f), the storage modulus of the SF ink increased significantly with the addition of high concentrations of potassium. This provided supporting data for the selection of an efficient coagulation agent and its working concentration [76]. To mimic the extrusion process, a three-step oscillation time sweep, including the initial state, extrusion process, and recovery, was used to measure the ink deconstruction and recovery properties (Fig. 5(g)) [46]. Fig. 5(h) shows the amplitude sweep of the SF-based printing ink used to assess the linear viscoelastic region (LVER). Within a LVER from 0.01% to 1% strains, the ink exhibited G′ predominantly over G″, indicating gel-like behavior. After the LVER, the ink began to deform permanently, and the crossover of G′ and G″ occurred when the ink began to flow like a liquid [77]. The gelation kinetics of the printing ink were assessed using the complex viscosity changes with different solidification methods, as shown in Fig. 5(i) [78]. In addition to the qualitative analysis mentioned above, a more recent study on the extrusion printing of silk/hydroxyapatite (HA) composites was performed by correlating the key linear and nonlinear viscoelastic properties to the geometric outcomes of printing. The study also proposed an estimation of ink printability by developing dedicated machine-learning algorithms based on linear and nonlinear rheological measurements [79].

5.2. Silk-based ME printing ink

ME is the most commonly used SF printing method. Unlike other printing methods with many ink requirements, ME facilitates

Table 3
SF-based extrusion printing strategies

Classifier	Ink Composition	Crosslinking type	Prototyping methodology/mechanism	References
Pure SF	SF	Physical	Induce regenerated SF aggregation (dehydration) with methanol by in situ structural transition of SF from random coil to β-sheet.	[71,80]
	SF	Physical	Direct the hierarchical assembly of SF with an aqueous bath containing inorganic salts.	[76]
	SF	Physical	One step gelation of SF through extrusion into nanoclay/PEG suspension.	[81]
Chemically modified SF	Methacrylated SF + methacrylated hollow mesoporous silica microcapsules	Physical and photocrosslinking	Self-assembly, photo-crosslinking and micro-particle covalent linkage	[82]
	SF-Norbornene	Physical and photocrosslinking	A weak and chemically crosslinked network was developed by conjugating norbornene to SF molecules and UV radiation for smooth extrusion, followed by ethanal treatment.	[83]
	SF–HRP and H_2O_2	Chemical	Form dityrosine bonds between tyrosine residues using HRP and partially crosslink SF to modulate ink viscosity for printing.	[84]
SF Hybrid	SF + gelatin	Physical	Gelatin acts as bulking agent that undergoes phase transition in physiological conditions.	[85,86]
	SF + tyramine-substituted gelatin	Physical	Temperature induced solidification and HRP mediated crosslinking.	[92]
	SF + collagen	Physical	Temperature induced solidification.	[87,88]
	SF + carrageenan	Physical	Temperature induced solidification.	[93]
	SF + silica	Physical	Sol–gel transition and self-assembly.	[94]
	SF + alginate	Ionic and photocrosslinking	Pregelatinized by the ionic cross-linking of alginate to increase the ink viscosity for extrusion printing, then photocrosslinking using riboflavin/sodium persulfate (SPS) system through oxidation of SF tyrosine residue.	[72]
	SF + alginate	Ionic	Ionic crosslinking of alginate with calcium ions and Pluronic F127	[89]
	SF + soy protein isolate	Photocrosslinking	Photocrosslinking using Riboflavin/SPS system through oxidation of SF tyrosine residue.	[95]
	SF + PEG	Physical	PEG induces β-sheet structure formation in SF structure and thus facilitates gelation in printing process.	[90]
	SF + Silica	Physical and chemical	Acid catalyzed crosslinking of the SF and simultaneous polycondensation of tetramethyl orthosilicate with 5-(trimethoxysilyl) pentanoic acid as a coupling agent.	[96]
SF particulate/ fibre composites	SF + OBC nanofibrils	Physical	SF backbone crosslinked by HRP/H_2O_2 and gel printing fidelity improved by addition of OBC.	[74]
	SF + Nanocellulose	Photocrosslinking	Photocrosslinking using riboflavin/ammonium persulphate system through oxidation of SF tyrosine residue.	[97]
	SF + hydroxypropyl methyl cellulose (HPMC)	Physical	Synergistic effects of hydrogen bonding and hydrophobic interaction between HPMC and SF molecules resulted in uniformly dispersed crosslinks composed of β-sheet structures.	[98]
	SF + carbon nanotubes	Physical	Molecular interactions between SF and carboxyl groups of carbon nanotubes result in structural increase of the β-sheet formation.	[99]
	SF + HA	Physical	Drying and setting of the high solid-content paste.	[91]
SF hybrid particle/fibre composites	SF + chitosan + cellulose nanoparticles	Physical	Interconnected network structures generated by the strong interactions between polymer chains and nano-fillers.	[100]
	SF + gelatin + glycerol + bacterial cellulose (BC)	Physical	BC to improve shape fidelity of SF/gelatin hydrogel	[101]
	SF + TA + $CaCl_2$ + rGO	Physical	The addition of $CaCl_2$ and nano reinforcement of rGO to SF–TA both increase the percentage of β-structures.	[73]
	SF + sodium alginate (SA) + HA	Physical	SA acting as a binder to form an injectable composite paste.	[102]
	SF + gelatin + HA + tricalcium phosphate	Physical	Gelatin acts as bulking agent that undergoes phase transition in physiological conditions, together with post-crosslinking treatment.	[103]

nearly any fluid to be extruded from a nozzle as long as the ink rheology is adjusted to the correct range. Herein, we review studies on SF-based extrusion printing based on different ink formulation strategies. We have categorized the SF extrusion printing cases into five major classifiers: Pure SF, chemically modified SF, pure SF solutions, SF hybrids, SF particulate/fiber composites, and SF hybrid particle/fiber composites. The detailed ink compositions, crosslinking types, and prototyping mechanisms are listed in Table 3.

A pure SF solution is frequently difficult to print directly with ME owing to its low viscosity. Only a few pure SF printing cases have been observed, which rely on in situ induction of the SF structural conformation using a methanol [71,80] or salt bath [76], or relying on a suspension printing methodology [81]. Chemical modification methods can be useful in imparting certain functionalities, such as photocrosslinking properties, to the printing process [82–84]. The SF hybrid is the most common strategy used in extrusion printing to modulate ink rheology or incorporate certain functionalities. Natural polymers (e.g., gelatin [85,86], collagen [87,88], and alginate [72,89]) and synthetic polymers (e.g., PEG [90]) are commonly mixed with SF for extrusion printing. Nanoparticles or fibers have also been observed to reinforce or functionalize the SF ink. For example, OBC nanofibrils have been observed to improve SF gel printing fidelity [74]. Bio-scaffolds printed with SF/HA ink exhibit enhanced bone-regeneration properties [91]. The SF hybrid particle/fiber composite is the last group fully utilizes hybrid printing and particle reinforcement.

Some representative ME-printed shapes are shown in Fig. 6. Zheng et al. [90] reported use of SF/PEG hydrogels as bioinks for 3D printing in tissue engineering (Fig. 6(a)). Blending PEG with SF induces silk β-sheet structure formation and thus gelation and water insolubility owing to physical crosslinking. These results

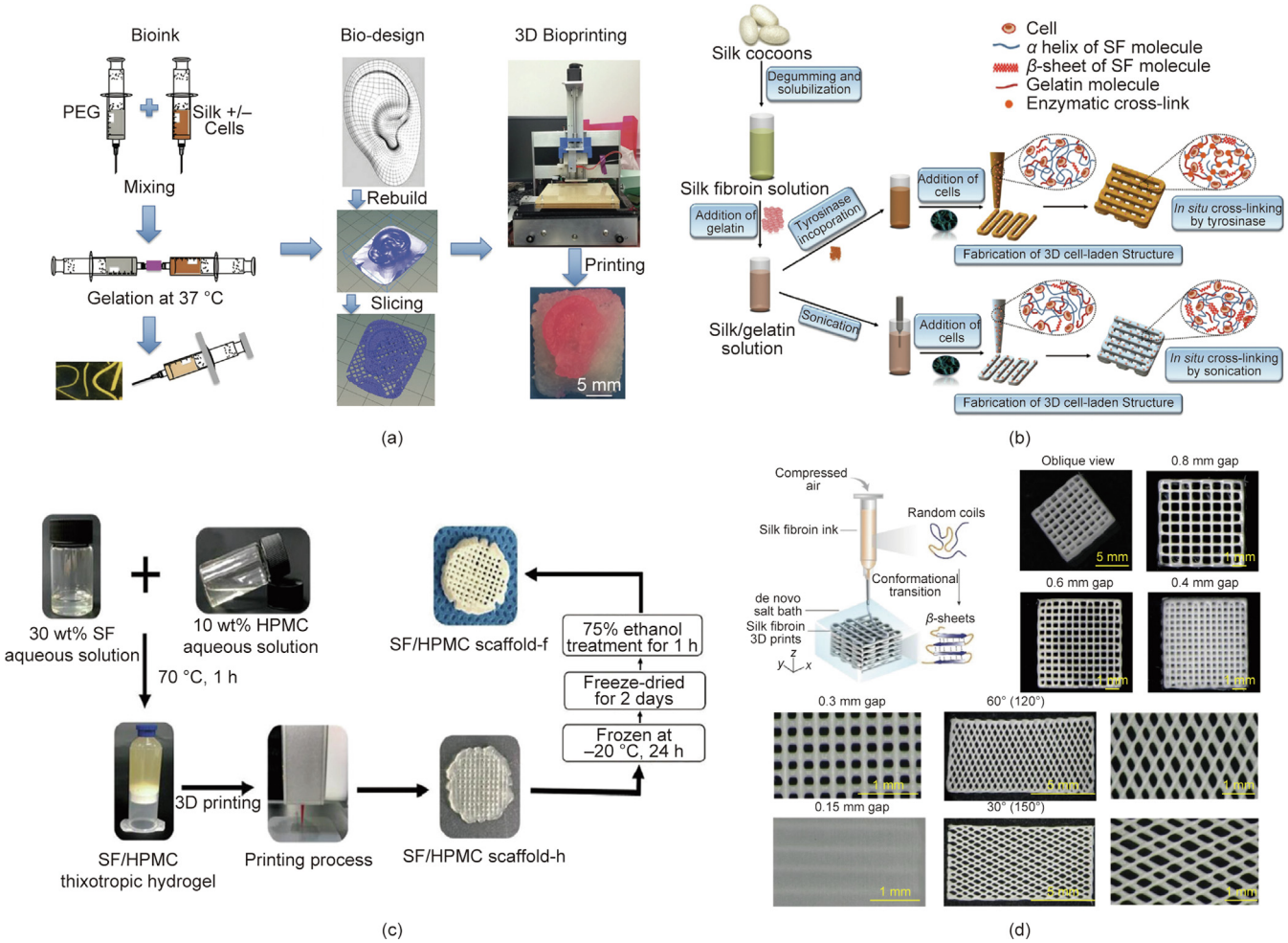

Fig. 6. (a) Schematic of the process of Silk/PEG bioink by 3D printing. Reproduced from Ref. [90] with permission of Wiley, ©2018. (b) Bio-printable and cell-laden SF-gelatin hydrogel. Reproduced from Ref. [78] with permission of Elsevier, ©2015. (c) Schematic representation of the process used to develop the SF/HPMC 3D scaffolds. Reproduced from Ref. [98] with permission of Sage Publications, ©2019. (d) Schematic of 3D printing with SF inks using a salt bath. Reproduced from Ref. [71] with permission of MDPI, ©2022.

suggest that the SF/PEG hydrogel provides a suitable environment for cell printing and function. Das et al. [78] developed a bio-printable, cell-laden SF-gelatin hydrogel (Fig. 6(b)). The gelation of the bio-ink was induced by enzymatic crosslinking using mushroom tyrosinase and physical crosslinking via sonication. Mechanistically, tyrosinases oxidize the accessible tyrosine residues of SF and gelatin in a three-step reaction. Sonication can aid in forming β-sheet formation within SF by accelerating the self-assembly of SF macromolecules. In this study, human nasal inferior turbinate tissue-derived mesenchymal progenitor cells were encapsulated and printed using this bio-ink, offering a new direction for the direct printing of tissue scaffolds in a patient-specific manner.

Zhong et al. [98] blended silk and HPMC as a bio-ink to print hydrogels for the regeneration of tracheal epithelia (Fig. 6(c)). The studies reported that the addition of HPMC changed the size of the β-sheet crystal structure and synergistically affected the gelation behavior to obtain a regenerated SF hydrogel with good mechanical properties. This is an excellent method of forming a hydrogel by incorporating additional polymers to induce the β-sheet structure of SF. Incorporating other natural polymers into the bio-ink can aids in lowering the temperature requirements during printing while providing support comparable to the extracellular matrix for the cells. Natural polymers such as chitosan, gelatin, and alginate have been demonstrated to undergo sol–gel transformations at physiological temperatures. However, these polymers exhibit poor mechanical properties. Crosslinking can occasionally be induced to increase the mechanical integrity of the prints. More recently, extrusion-based SF printing using a concentrated SF solution with a salt-bath coagulation system has been reported (Fig. 6(d)) [71]. The paper revealed excellent printing resolution with printed high-aspect-ratio structures, such as a cantilever with only one supported end.

Owing to the material versatility and flexibility in the prototyping methodology design, ME has several noticeable limitations. For example, the printing resolution is frequently low depending on the nozzle size. Furthermore, a compromise between printing resolution and nozzle clogging is set to ensure a smooth extrusion process. The printing geometry is still limited to basic shapes because complex shapes, particularly those with overhangs, have a high requirement for the self-supporting ability of the material, which is difficult to achieve for materials with low moduli, such as SF hydrogels. In addition, printed structures often lack mechanical integrity owing to the poor adhesion between the printing layers.

6. Vat polymerization

6.1. Printing mechanism and ink requirements

Unlike MJ and ME, in which bioinks are deposited in designated areas, VP is a light-assisted printing technique. Most SF-based VP

printing studies use DLP as the printing technique. As a projection-based printing technique, DLP prints a part by illuminating a photocurable resin with a 2D pixelated pattern. When one layer of resin is cured, the platform drops a certain distance and repeatedly solidifies the material layer-by-layer until a solid 3D object is generated [104]. The curing kinetics of the VP printing process can be complex; however, a semi-empirical equation adapted from the Beer–Lambert equation can be used to describe the curing process [105]:

$$C_d = D_p \ln\left(\frac{E}{E_c}\right) \tag{6}$$

where C_d is the curing depth; D_p is the light penetration depth; E and E_c are the irradiation dose and critical energy, respectively. Thus, the curing depth C_d is determined by both the optical properties (D_p and E_c) of the bioink and the printer setting of the irradiation dose E. The optical properties of the bioink are directly affected by the printing ink formulation, polymer concentration, and photoinitiator concentration [106]. For proper curing of the bioink, E must exceed E_c [107].

For commercial resins, such as acrylic resins, strength is frequently not a significant problem because of their highly crosslinked structures. However, for bioresins, such as SF hydrogels, whose strength at the gelling point is low, excess energy E_x is proposed to increase the gelling strength of the hydrogel material and is defined as:

$$E_x = E_c\left(\frac{D_p}{C_d}\right)\left\{\exp\left(\frac{C_d}{D_p} - 1\right) - 1\right\} \tag{7}$$

Excess energy E_x is positively correlated with E_c and negatively correlated with C_d. Typically, for VP printing, the bioink comprises a polymer or monomer, photoinitiator, and light absorber/photoinhibitor. While polymers, monomers, and photoinitiators are the major components of the photocrosslinking reaction, the light absorber competes with the photoinitiator for photons to attenuate light [107]. Light absorbers reduce structural bleeding by mitigating the free-radical migration distance, which is particularly useful when printing geometries with high aspect ratios [108,109]. Commonly investigated light absorbers include synthetic or natural food dyes, inorganic particles, and pigments. UV blockers used in sunscreen also have the potential to be used as light absorbers. Meanwhile, some UV absorbers such as dyes can impart specific functional properties on printed constructs, such as tunable surface wettability and permeability, mechanical property modulation, light emission, and mechanochromic features [110]. However, these factors have not been exclusively investigated [107]. Thus, an investigation of ink formulations is required to achieve constructs with optimum resolution and adequate green part strength.

The ink viscosity is also detrimental to the VP printing process because it affects the curing rate, curing depth, green part strength, oxygen inhibition, and peeling force after one-layer printing. As opposed to ME, the desired viscosity for VP is low: 1–10 Pa·s [107]. This is because a high ink viscosity may result in bubbles in the ink vat, difficulty in peeling, and insufficient ink coating between the layers. In summary, the VP printing bioinks require:

① Good photo crosslinking characteristics, including fast crosslinking rate and high crosslinking strength;

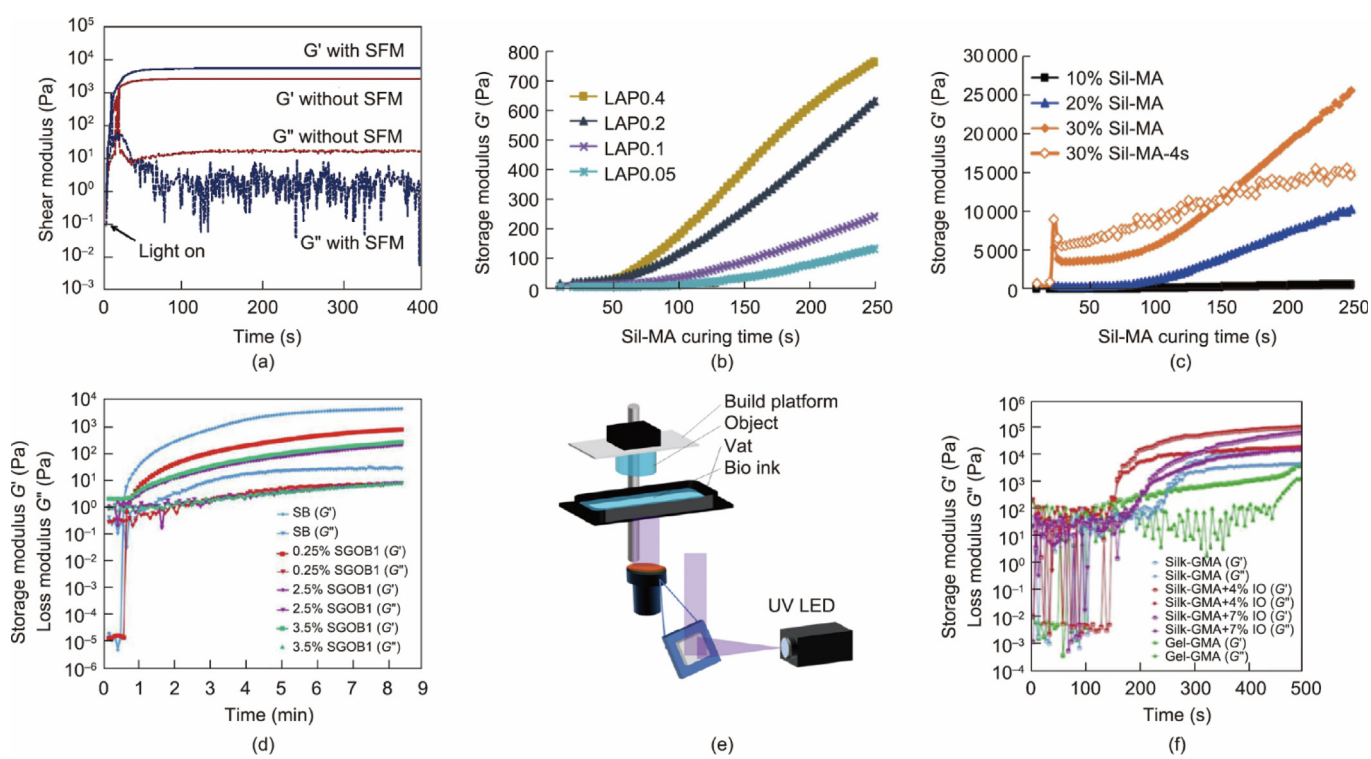

Fig. 7. (a) Rheological behavior of PEG4A bioinks with SFM by in situ photorheometry. Reproduced from Ref. [112] with permission of American Chemical Society, ©2018. (b–c) In situ rheology during UV exposure. The effect of LAP contents and Sil-MA contents on the G′ during UV exposure. Reproduced from Ref. [113] with permission of Springer Nature, ©2018. (d) Graph of storage and loss moduli of SGOB1 bioinks as a function of time under UV exposure (14.1 mW·cm^{-2}). Reproduced from Ref. [114] with permission of American Chemical Society, ©2020. (e) Schematic diagram of light curing printing (DLP) mechanism. Bioink-added photoinitiator was printed in a layer-by-layer style with DLP printer. Reproduced from Ref. [116] with permission of Wiley, ©2021. (f) Rheological determination of gelling points of gelatin-meth acrylate (GelMA) and Sil-MA with different additives. Reproduced from Ref. [115] with permission of IOP Publishing, ©2021.

② Good fluidity and low viscosity, which contrast the demands for extrusion printing;

③ Appropriate curing kinetics.

Light curing and finalization should be completed before the platform action; therefore, the curing kinetics should be carefully adjusted, and it is important to select a suitable photoinitiator [109,111].

Rheological evaluation is a prerequisite for the development of printable inks that can improve printing quality. Representative photocuring rheological characteristics of the SF-based ink are presented in Fig. 7. Shin et al. [112] studied the rheological properties of a 4-am polyethylene glycol acrylate (PEG4A) precursor solution containing SF incorporated with melanin nanoparticles (SFM), as shown in Fig. 7(a). Immediately the light was irradiated, the G′ of the precursor solution containing SFM biological ink increased rapidly and reached a plateau, indicating that the gelation process took place very quickly and was completed within 1 min. Kim et al. [113] adjusted the rheological properties by changing the content of the photoinitiator and Sil-MA, as shown in Figs. 7(b) and (c). An SF-based bioink (Sil-MA) was produced through methacrylation by adding glycidyl methacrylate to the SF solution. The results showed that the curing kinetics increased with increasing LAP and Sil-MA content. With an increase in the UV curing time, Sil-MA hydrogels tended to become stiffer, probably because of the formation of a more stable hydrophobic domain. Ajiteru et al. [114] covalently rGO with glycidyl methacrylated SF to prepare a bioink (SGOB1). As shown in Fig. 7(d), the bioink was entirely polymerized after 4 s of UV irradiation. Photorheology was also used to assess the gelling strength. As shown in Fig. 7(f), the complete gelling time was assessed for Sil-MA with different additives [115]. In summary, VP bioinks generally exhibit a good flow performance and low viscosity before the photocuring reaction. Upon light irradiation, the ink can be rapidly crosslinked and quickly solidified into a solid/gel state with a higher modulus.

6.2. Silk-based VP printing ink

We also classified SF-based VP printing strategies into four main groups based on the ink formulations: pure SF, SF hybrid, Sil-MA, and Sil-MA hybrid (Table 4). Another distinct characteristic could also be the photoinitiator used. Three types of photoinitiators are primarily used for SF-based VP printing: riboflavin, eosin Y and lithium phenyl-2,4,6-trimethylbenzoyl phosphonate (LAP). The first two are photooxidation reactions, and the last is methacryloyl-based free radical irradiation. A more detailed explanation of SF photocrosslinking strategies is provided in a published review paper [117].

Compared with other printing methods, VP techniques are straightforward and easier to operate. More importantly, they offer excellent printing accuracy and reliable reproducibility of the SF printing materials, as shown in Fig. 8. Therefore, much effort has been devoted to printing SF using the VP method. The tyrosine contained in the SF molecule, whose phenolic hydroxyl group, can be crosslinked by the initiator under visible-light conditions to form dityrosine and then a crosslinking network. Shin et al. [118] fabricated SF microneedles by the DLP 3D printing of an SF solution with riboflavin as the enzymatic photoinitiator (Fig. 8(a)). The SF microneedle was robust and demonstrated no severe damage to the structure upon the application of a compressive stress of ~300 mN. They also obtained a hydrogel with excellent structural stability by adding gelatin to the SF ink owing to the additional crosslinking points using DLP 3D printing [120].

The inclusion of photosensitive polymers in the SF ink is another method for developing VP printing ink. Kwak et al. [122] used SF incorporated PEG4A as a bioink for the 3D printing of DLP (Fig. 8(b)). They observed that the incorporation of biocompatible SF particles enhanced the mechanical properties of the SF hydrogel and provided elasticity for the generation of artificial skin. The SF-PEG4A hydrogel embedded with fibroblasts generated a thicker keratin layer than the pure PEG4A hydrogel. They also added SF particles to GelMA as a bioink for DLP 3D printing. The cells encapsulated in the structure showed high levels of metabolic activity, indicating that SF-GelMA is a biocompatible material [121].

Although the VP printing technique has the advantages of rapid printing speed, high resolution, realization of highly complex structures, and biocompatible nozzle-free printing methodology, it is still not widely adopted, primarily because of the limited number of photosensitive materials that can be applied. Therefore, novel bioinks that are biodegradable, biocompatible, printable, and mechanically stable must be developed. In 2019, Kim et al. [113] synthesized a bioink generated from SF for DLP 3D bioprinting, targeting tissue-engineering applications (Fig. 8(c)). The Sil-MA hydrogel fabricated using DLP showed outstanding biocompatibility as well as mechanical and rheological properties. This could be a superior bioink for DLP printing in biological and clinical applications.

To fabricate 3D structures using Sil-MA via DLP 3D printing, Ajiteru et al. [114] fabricated a DLP-printable bioink through the covalent reduction of GO by glycidyl methacrylated SF (Fig. 8(d)). These hydrogels exhibit superior mechanical, electroconductive, and neurogenic properties. Ajiteru et al. [115] developed a magnetic bioreactor system and magnetic hydrogel by single-stage 3D printing using the DLP technique for the differentiation of myoblast cells. The 3D-printed magnetic bioreactor system provides a

Table 4
SF-based VP printing strategies.

Classifier	Ink Composition	Photo initiator	Prototyping mechanism	References
Pure SF	SF	Riboflavin	The phenolic photocrosslinking between SF molecules.	[118]
	SF	Ruthenium (Ru)/SPS	The phenolic photocrosslinking between SF molecules	[119]
SF Hybrid	SF + Gelatin	Riboflavin	The phenolic photocrosslinking between SF and gelatin.	[120]
	SF + GelMA	Eosin Y	The modification of gelatin with pendant methacrylate groups can carry out chemical crosslinking under the UV.	[121]
	SF + PEG4A	Eosin Y	The crosslinking reaction occurred between the acryl functional groups of PEG4A molecules by irradiation.	[112,122]
	SF + PEGDMA	LAP	The crosslinking reaction occurred between the methacrylate groups of PEGDMA molecules.	[116]
Sil-MA	Sil-MA	LAP	The vinyl double bonds on GMA of Sil-MA could react with each other intra-chain or between chains under the UV.	[113,123-125]
Sil-MA Hybrid	Sil-MA + GO	LAP	Similar with Sil-MA	[114]
	Sil-MA + GelMA + iron oxide (IO)	LAP	The crosslinking between The GMA group of Sil-MA and the MA group of GelMA	[115]

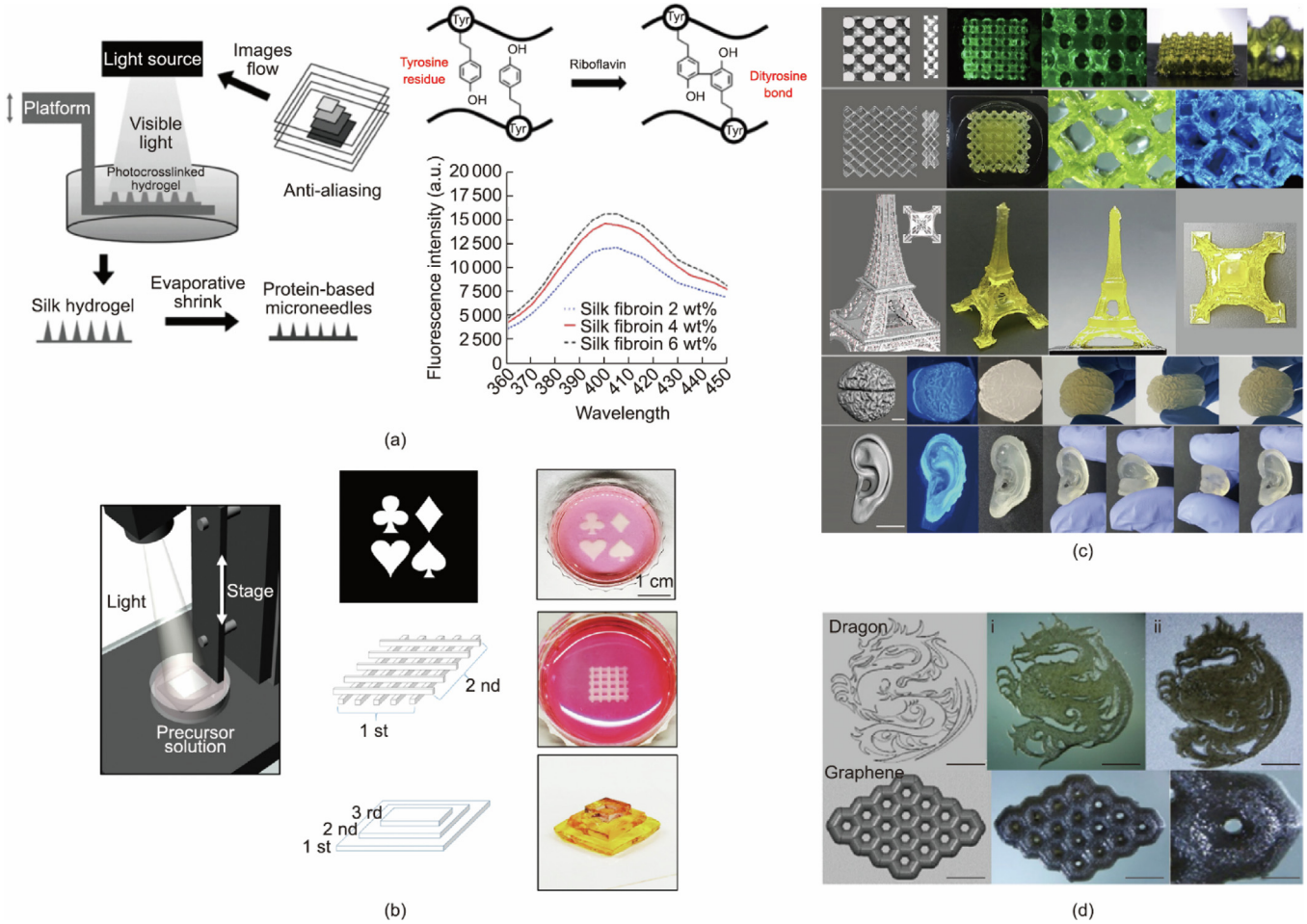

Fig. 8. (a) DLP 3D printing of SF microneedles using SF ink. Reproduced from Ref. [118] with permission of Elsevier, ©2021. (b) DLP 3D printing of SF-PEG precursor solution in a visible range of light. Reproduced from Ref. [122] with permission of Elsevier, ©2019. (c) Printability of 30% Sil-MA using DLP printer. A porous scaffold and Eiffel Tower imitation. Reproduced from Ref. [113] with permission of Springer Nature, ©2018. (d) Dragon logo and 3D molecular structure of graphene using 2.5% SGOB1 bioink. Reproduced from Ref. [114] with permission of American Chemical Society, ©2020.

suitable 3D environment for myoblast cells to further differentiate into silk magnetic composite hydrogels.

7. Promising strategies for 3D printing SF

7.1. Technique aspect

7.1.1. Emerging photopolymerization techniques

Although most silk-based printing studies rely on extrusion-based printing methods, VP printing techniques have shown enormous potential in the biomedical field because of their superior printing quality and speed. Recently, emerging VP techniques such as two-photon/multiphoton polymerization (2PP) and volumetric additive manufacturing (VAM) have shed light on this field.

Among the various VP techniques, stereolithographic appearance (SLA) was first developed in the early 1980s [126]. As shown in Fig. 9(a), a laser beam was emitted by the laser source to cure one layer of photopolymer resin onto the build platform in a point-wise manner. Eventually, the entire object was printed layer by layer through the movement of the platform and lifted from the liquid resin. The relative positions of the light source and vat can be altered depending on the printer configuration [127]. Using a mechanism similar to that of SLA, DLP uses a projector to project UV light onto the resin surface such that the entire resin layer can be cured simultaneously (Fig. 9(b)). Compared with the dot-wise printing of SLA, the layer-wise printing characteristic of DLP offers higher efficiency. Building on this, another fast and continuous printing method, continuous CLIP, has recently been developed [128]. In traditional VP methods, oxygen inhibition causes incomplete polymerization and surface tackiness. Introducing a thin layer of liquid resin ("dead zone") between the projecting window and printed surface solved the issues of superb surface finish and faster printing speed.

Despite all the developments in VP printing techniques and being the most precise method, the lateral resolution is around 10–50 μm for the aforementioned VP techniques [129]. In comparison, 2PP holds promise for printing nanosized features with a high lateral resolution of approximately 100 nm [130,131]. Since the two-photon absorption of light with wavelength of λ would intrigue a tightly focused voxel area with a volume of λ^3, the initiated polymerization area is much smaller in 2PP compared with traditional photopolymerization (Fig. 9(c)) [132,133]. Furthermore, a more recent study developed a volume-based printing methodology by concurrently printing all points within an object through a rotating-illumination system (Fig. 9(d)), offering another significant leap in printing speed and surface finish.

3D printing is a rapidly developing field for achieving maximized printing resolution and speed, which can be seen particularly in the various VP techniques that have emerged in recent years, from the earliest SLA, 2PP, to DLP, CLIP, and the most recent VAM. However, from the printing material point of view, the

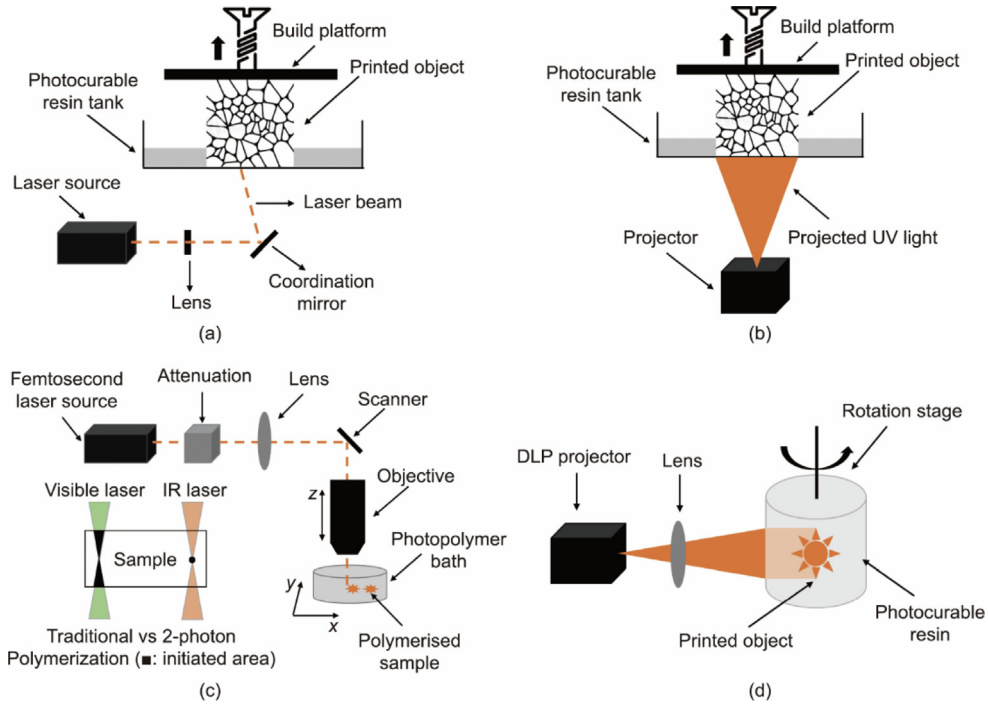

Fig. 9. Schematics of different VP processes. (a) SLA, (b) DLP, (c) 2PP. (d) VAM.

VP-based printing technique has no significant effect on the material properties. Currently, DLP is the predominant technique used to print SF-based inks, as summarized in Section 6. When more advanced techniques are introduced in SF printing, there will be vast potential for achieving SF-based printed structures with a greater level of complexity and functionality.

7.1.2. Four-dimensional printing

Four-dimensional (4D) printing is a result of the rapid development of printing techniques, designs, and multidisciplinary smart materials. It has attracted great interest in various fields since its conceptualization in 2013 [134]. Compared with 3D printing, one more dimension of "time" is involved, which means the 3D printed part changes its configuration, property or certain functionality along with the time when exposed to external stimuli such as heat, light, water, pH, and so forth [135]. Thus, it can be used to create materials with self-healing and self-folding properties, or on-demand shape transformations from one shape to another [136]. Such properties can be beneficial in various fields such as self-healing batteries in the case of an accident and bio-scaffolds with shape memory capabilities [137]. Meanwhile, 4D printing is achievable using the most commonly used 3D printing techniques, such as ME and VP. Printing material systems include shape-memory polymers, liquid-crystal elastomers, and composite hydrogels [135].

Very few SF-based 4D printing studies have been conducted at its infancy stage. In one study, a shape-morphing Sil-MA hydrogel was fabricated using DLP printing [138]. Shape-morphing was achieved by changing the exterior or interior properties of the Sil-MA hydrogel under physiological conditions. A tracheal–mimetic tissue structure was prepared using this technique, and the *in vivo* results suggested the potential value of such a 4D bio-printing system for biomedical applications (Fig. 10). In another study, a tendril-like structure was printed with graphene nanoplatelets-modified SF as the core and PHBV as the shell. The fourth dimension of motion is realized by the different thermal expansion coefficients of the two materials and the conversion of thermal energy into mechanical actuation [138]. Thus, taking this initial step forward, there is vast potential to transfer the unique properties of SF into 4D printed objects that are "smart or alive" for applications in various fields. Apart from the shape-morphing structures mentioned above, stimuli-responsive drug delivery is a promising application field for 4D printing SF material.

7.2. Material aspect

7.2.1. Promising SF gelation methods

Despite advances in the progress of SF-based hydrogels, recent methods for SF gelation, including sonication, pH adjustment, and the use of organic solvents, have apparent limitations, such as non-physiological conditions, lack of reversible crosslinking, and weak mechanical properties [139]. Specifically, the absence of dynamic sacrificial bonds in the network to efficiently dissipate energy at the molecular level limits the recapitulation of outstanding toughness *in vitro*; therefore, most are affected by brittle behavior. Incorporating a dynamic energy dissipation mechanism into the physical interconnection network may be an effective strategy for enhancing the mechanical properties of regenerated SF-based hydrogels. Shi et al. [14] developed a dynamic metal-ligand coordination chemistry strategy to assemble SF-based hydrogels between SF microfibers and a polysaccharide binder under physiological conditions. The obtained SF-based hydrogels exhibited outstanding shear-thinning and self-healing properties, thereby enabling the filling of irregularly shaped tissue defects without gel fragmentation. In another study, Huang et al. [140] grafted cholesterol or β-cyclodextrin onto the carboxylated SF. The two chemically modified SF were assembled into an SF-based hydrogel via host-guest interactions. Compared with conventional SF hydrogels, the presented hydrogel showed higher mechanical strength, toughness, and suitable self-healing properties without external stimuli. These results reveal that the dynamic crosslinking of SF-based hydrogels is a promising novel generation of 3D printing SF materials.

7.2.2. Chemical modification methods

In recent years, research on SF chemistry has primarily focused on understanding the molecular structures and structural property

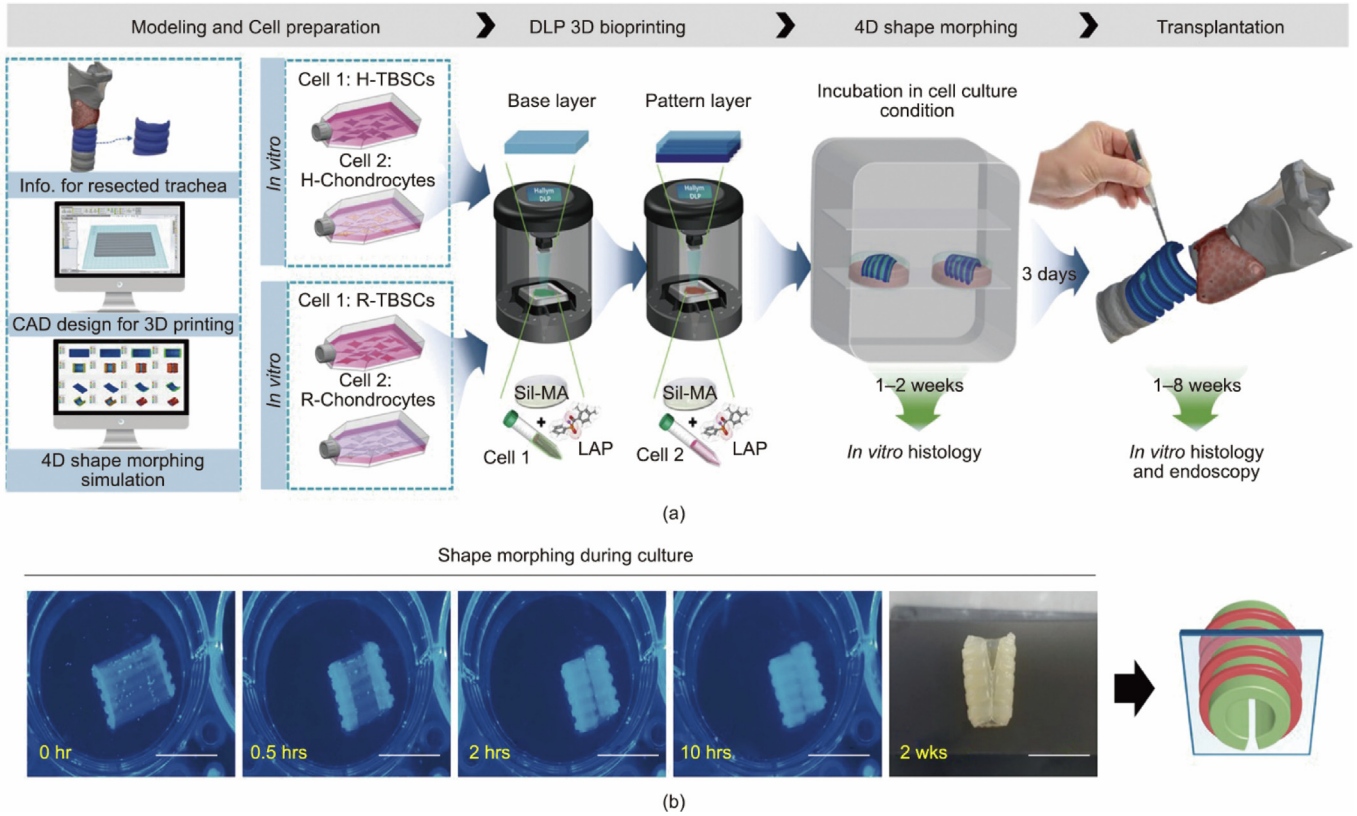

Fig. 10. (a) Schematic of the 4D-bioprinted silk hydrogels for tissue engineering application process; (b) in vitro culture of 4D-bioprinted Sil-MA trachea with shape morphing properties (Scale bars, 1 cm). Reproduced from Ref. [125] with permission of Elsevier, ©2020.

relationships of native SF and developing advanced techniques for processing SF into functional materials [141]. However, studies on the chemical modification of SF have been limited to obtaining rationally designed physicochemical and biological properties. To promote SF research and expand its applications in 3D printing, it is crucial to develop chemical tools for modifying the molecular structure of SF for the precise tailoring of material properties to meet application needs. Moreover, the preparation of silk-based fine chemicals with precise structures, functions, and high added value has attracted increasing interest and potential, particularly in the fields of biomedicine and cosmetics. From a chemical perspective, silk proteins are biopolymers composed of amino acids, including serine, threonine, tyrosine, glutamic acid, aspartic acid, lysine, and arginine, which have several reactive groups (hydroxyl, carboxyl, and amino groups). The most abundant reactive groups were serine (12.1%) and tyrosine (5.3%) and the rest of the reactive groups are less than 1% [142]. There is a vast potential to develop silk materials with good printability and mechanical properties for 3D printing through reactions between the reactive groups of SF and other molecules. Recently, a study introduced an esterification method to modify SF using succinic anhydride in an ionic liquid/dimethylformamide homogeneous solution and achieved controlled SF carboxylation with less protein degradation [143]. This strategy promises to become a novel SF-based material for 3D printing.

8. Conclusions and prospects

Silk-based protein materials have attracted significant interest for the formulation of 3D printing bioinks owing to their processing flexibility, mechanical integrity, cytocompatibility, controllable biodegradability, and immune tolerance. From the statement of the mainstream 3D printing techniques according to the ISO/ASTM 52900 standard to the illustration of the chemical and structural characteristics of the silk material, we discuss the adaptability of the silk material in each printing technique. The focus was then on MJ, ME, and VP, which are the most frequently used techniques. Comparing the printing mechanism, ink requirements, and silk printing structures with the three different techniques, MJ printed precise but 2D structures that are frequently attached onto a substrate, ME was the most widely adopted technique owing to its material flexibility but presented relatively low printing resolution and shape fidelity, and VP held the promise of manufacturing structures with both high resolution and complexity; however, there is a major lack of silk-based printing material for the VP process. We also propose promising strategies from both technical and material aspects for prototyping highly precise and functional tissue engineering scaffolds or devices from silk-based materials to broaden their applications in biomimetic tissue structures such as vasculatures, highly precise biomedical devices such as microneedles, and personalized medicine.

Acknowledgement

We acknowledge the funding support from National Natural Science Foundation of China (51873134, 52303043), Natural Science Foundation of Jiangsu Province of China (BK20211317), The Natural Science Foundation of the Jiangsu Higher Education Institutions of China (23KJB430031), Priority Academic Program Development of Jiangsu Higher Education Institutions (PAPD), China National Textile and Apparel Council Key Laboratory for Silk Functional Materials and Technology, Opening Project of Key Lab-

oratory of Jiangsu Province for Silk Engineering (KJS2168), Soochow University. We would like to thank Editage for English language editing.

Compliance with ethics guidelines

Xiaoliang Cui, Jun Zhang, Yan Qian, Siqi Chang, Benjamin J. Allardyce, Rangam Rajkhowa, Hui Wang and Ke-Qin Zhang declare that they have no conflict of interest or financial conflicts to disclose.

References

[1] Guo N, Leu MC. Additive manufacturing: technology, applications and research needs. Front Mech Eng 2013;8(3):215–43.
[2] Song Y, Yan Y, Zhang R, Xu D, Wang F. Manufacture of the die of an automobile deck part based on rapid prototyping and rapid tooling technology. J Mater Process Technol 2002;120(1–3):237–42.
[3] Vilaro T, Abed S, Knapp W. Direct manufacturing of technical parts using selective laser melting: example of automotive application. In: Proceedings of 12th European Forum on Rapid Prototyping; 2008 Mar 5–6; Paris, France. Massachusetts: French Rapid Prototyping and additive manufacturing Association (AFPR); 2008.
[4] Giannatsis J, Dedoussis V. Additive fabrication technologies applied to medicine and health care: a review. Int J Adv Manuf Technol 2009;40(1–2):116–27.
[5] Sachlos E, Czernuszka J. Making tissue engineering scaffolds work. Review: the application of solid freeform fabrication technology to the production of tissue engineering scaffolds. Eur Cell Mater 2003;5:29–40.
[6] Moroni L, Burdick JA, Highley C, Lee SJ, Morimoto Y, Takeuchi S, et al. Biofabrication strategies for 3D *in vitro* models and regenerative medicine. Nat Rev Mater 2018;3(5):21–37.
[7] Chen Y, Zhang J, Liu X, Wang S, Tao J, Huang Y, et al. Noninvasive *in vivo* 3D bioprinting. Sci Adv 2020;6(23):eaba7406.
[8] Kyle S, Jessop ZM, Al-Sabah A, Whitaker IS. 'Printability' of candidate biomaterials for extrusion based 3D printing: state-of-the-art. Adv Healthc Mater 2017;6(16):1700264.
[9] Kundu S, editor. Silk biomaterials for tissue engineering and regenerative medicine. Amsterdam: Elsevier; 2014.
[10] Kundu B, Rajkhowa R, Kundu SC, Wang X. Silk fibroin biomaterials for tissue regenerations. Adv Drug Deliv Rev 2013;65(4):457–70.
[11] Yang Y, Chen X, Ding F, Zhang P, Liu J, Gu X. Biocompatibility evaluation of silk fibroin with peripheral nerve tissues and cells *in vitro*. Biomaterials 2007;28(9):1643–52.
[12] Hofmann S, Hagenmüller H, Koch AM, Müller R, Vunjak-Novakovic G, Kaplan DL, et al. Control of *in vitro* tissue-engineered bone-like structures using human mesenchymal stem cells and porous silk scaffolds. Biomaterials 2007;28(6):1152–62.
[13] Singh YP, Bhardwaj N, Mandal BB. Potential of agarose/silk fibroin blended hydrogel for *in vitro* cartilage tissue engineering. ACS Appl Mater Interfaces 2016;8(33):21236–49.
[14] Shi L, Wang F, Zhu W, Xu Z, Fuchs S, Hilborn J, et al. Self-healing silk fibroin-based hydrogel for bone regeneration: dynamic metal-ligand self-assembly approach. Adv Funct Mater 2017;27(37):1700591.
[15] Rodriguez MJ, Brown J, Giordano J, Lin SJ, Omenetto FG, Kaplan DL. Silk based bioinks for soft tissue reconstruction using 3-dimensional (3D) printing with in vitro and in vivo assessments. Biomaterials 2017;117:105–15.
[16] Park SY, Ki CS, Park YH, Jung HM, Woo KM, Kim HJ. Electrospun silk fibroin scaffolds with macropores for bone regeneration: an *in vitro* and *in vivo* study. Tissue Eng Part A 2010;16(4):1271–9.
[17] Zhang W, He J, Li X, Liu Y, Bian W, Li D, et al. Fabrication and *in vivo* implantation of ligament–bone composite scaffolds based on three-dimensional printing technique. Chin J Repar Reconstr Surg 2014;28(3):314–7. Chinese.
[18] Melke J, Midha S, Ghosh S, Ito K, Hofmann S. Silk fibroin as biomaterial for bone tissue engineering. Acta Biomater 2016;31:1–16.
[19] Chen CH, Liu J, Chua CK, Chou SM, Shyu V, Chen JP. Cartilage tissue engineering with silk fibroin scaffolds fabricated by indirect additive manufacturing technology. Materials 2014;7(3):2104–19.
[20] Bhardwaj N, Nguyen QT, Chen AC, Kaplan DL, Sah RL, Kundu SC. Potential of 3-D tissue constructs engineered from bovine chondrocytes/silk fibroin–chitosan for *in vitro* cartilage tissue engineering. Biomaterials 2011;32(25):5773–81.
[21] Vepari C, Kaplan DL. Silk as a biomaterial. Prog Polym Sci 2007;32(8–9):991–1007.
[22] Seo YK, Yoon HH, Song KY, Kwon SY, Lee HS, Park YS, et al. Increase in cell migration and angiogenesis in a composite silk scaffold for tissue-engineered ligaments. J Orthop Res 2009;27(4):495–503.
[23] ISO/ASTM 52900:2015E: Standard terminology for additive manufacturing–general principles–terminology. ISO and ASTM standard. New York: the World Trade Organization Technical Barriers to Trade (TBT) Committee; 2015.
[24] Wohlers T, Campbell RI, Huff R, Diegel O, Kowen J. 3D printing and additive manufacturing state of the industry 2019 Wohlers Report. Report. Colorado: Wohlers Associates; 2019.
[25] Zhang J, Allardyce BJ, Rajkhowa R, Wang X, Liu X. 3D printing of silk powder by binder jetting technique. Addit Manuf 2021;38:101820.
[26] Thilagavathi G, Viju S. Silk as a suture material. In: Advances in Silk Science and Technology. Cambridge: Woodhead Publishing; 2015. p. 219–32.
[27] Huang Y, Sun G, Lyu L, Li Y, Li D, Fan Q, et al. Dityrosine-inspired photocrosslinking technique for 3D printing of silk fibroin-based composite hydrogel scaffolds. Soft Matter 2022;18(19):3705–12.
[28] Luo K, Yang Y, Shao Z. Physically crosslinked biocompatible silk-fibroin-based hydrogels with high mechanical performance. Adv Funct Mater 2016;26(6):872–80.
[29] Chao PHG, Yodmuang S, Wang X, Sun L, Kaplan DL, Vunjak-Novakovic G. Silk hydrogel for cartilage tissue engineering. J Biomed Mater Res B Appl Biomater 2010;95B(1):84–90.
[30] Kim UJ, Park J, Li C, Jin HJ, Valluzzi R, Kaplan DL. Structure and properties of silk hydrogels. Biomacromolecules 2004;5(3):786–92.
[31] Rnjak-Kovacina J, Wray LS, Burke KA, Torregrosa T, Golinski JM, Huang W, et al. Lyophilized silk sponges: a versatile biomaterial platform for soft tissue engineering. ACS Biomater Sci Eng 2015;1(4):260–70.
[32] Silva SS, Motta A, Rodrigues MT, Pinheiro AF, Gomes ME, Mano JF, et al. Novel genipin-cross-linked chitosan/silk fibroin sponges for cartilage engineering strategies. Biomacromolecules 2008;9(10):2764–74.
[33] Lu S, Wang X, Lu Q, Zhang X, Kluge JA, Uppal N, et al. Insoluble and flexible silk films containing glycerol. Biomacromolecules 2010;11(1):143–50.
[34] Gupta MK, Khokhar SK, Phillips DM, Sowards LA, Drummy LF, Kadakia MP, et al. Patterned silk films cast from ionic liquid solubilized fibroin as scaffolds for cell growth. Langmuir 2007;23(3):1315–9.
[35] Allardyce BJ, Atlas M, Dilley R, Wang X. Silk films as a repair material for perforations of the tympanic membrane. In: Allardyce B, Rajkhowa R, Atlas MD, Dilley RJ, Wang X, editors. Proceedings of the 89th Textile Institute World Conference. Wuhan, China. Tokyo: Fiber Society; 2014. p. 6–10.
[36] Yu Z. SF/chitosan scaffold material for liver tissue engineering [dissertation]. Beijing: Tsinghua University; 2009.
[37] Lotz B, Colonna CF. The chemical structure and the crystalline structures of *Bombyx mori* silk fibroin. Biochimie 1979;61(2):205–14.
[38] Zhou CZ, Confalonieri F, Jacquet M, Perasso R, Li ZG, Janin J. Silk fibroin: structural implications of a remarkable amino acid sequence. Proteins 2001;44(2):119–22.
[39] Zhou CZ, Confalonieri F, Medina N, Zivanovic Y, Esnault C, Yang T, et al. Fine organization of *Bombyx mori* fibroin heavy chain gene. Nucleic Acids Res 2000;28(12):2413–9.
[40] Xu G, Gong L, Yang Z, Liu XY. What makes spider silk fibers so strong? From molecular-crystallite network to hierarchical network structures. Soft Matter 2014;10(13):2116–23.
[41] Drummy LF, Farmer BL, Naik RR. Correlation of the beta-sheet crystal size in silk fibers with the protein amino acid sequence. Soft Matter 2007;3(7):877–82.
[42] Hodgkinson T. Silk fibroin biomaterials for skin tissue engineering applications [dissertation]. Manchester: University of Manchester; 2014.
[43] Valluzzi R, Gido SP, Muller W, Kaplan DL. Orientation of silk III at the air–water interface. Int J Biol Macromol 1999;24(2–3):237–42.
[44] Zhang J, Allardyce BJ, Rajkhowa R, Zhao Y, Dilley RJ, Redmond SL, et al. 3D printing of silk particle-reinforced chitosan hydrogel structures and their properties. ACS Biomater Sci Eng 2018;4(8):3036–46.
[45] Zhang J, Allardyce BJ, Rajkhowa R, Kalita S, Dilley RJ, Wang X, et al. Silk particles, microfibres and nanofibres: a comparative study of their functions in 3D printing hydrogel scaffolds. Mater Sci Eng C 2019;103:109784.
[46] Zhang R, Tao Y, Xu Q, Liu N, Chen P, Zhou Y, et al. Rheological and ion-conductive properties of injectable and self-healing hydrogels based on xanthan gum and silk fibroin. Int J Biol Macromol 2020;144:473–82.
[47] Vyas C, Zhang J, Øvrebø Ø, Huang B, Roberts I, Setty M, et al. 3D printing of silk microparticle reinforced polycaprolactone scaffolds for tissue engineering applications. Mater Sci Eng C 2021;118:111433.
[48] Umar M, Li WY, Bonacchini GE, Min K, Arif S, Omenetto FG, et al. Inkjet-printed lasing silk text on reusable distributed feedback boards. Opt Mater Express 2020;10(3):818–30.
[49] Ma L, Patil A, Wu R, Zhang Y, Meng Z, Zhang W, et al. A capacitive humidity sensor based on all-protein embedded with gold nanoparticles @ carbon composite for human respiration detection. Nanotechnology 2021;32(19):19LT01.
[50] DeBari MK, Keyser MN, Bai MA, Abbott RD. 3D printing with silk: considerations and applications. Connect Tissue Res 2020;61(2):163–73.
[51] Tan XH, Liu L, Mitryashkin A, Wang YY, Goh JCH. Silk fibroin as a bioink—a thematic review of functionalization strategies for bioprinting applications. ACS Biomater Sci Eng 2022;8(8):3242–70.
[52] Rider P, Zhang Y, Tse C, Zhang Y, Jayawardane D, Stringer J, et al. Biocompatible silk fibroin scaffold prepared by reactive inkjet printing. J Mater Sci 2016;51(18):8625–30.
[53] Antic A, Zhang J, Amini N, Morton D, Hapgood K. Screening pharmaceutical excipient powders for use in commercial 3D binder jetting printers. Adv Powder Technol 2021;32(7):2469–83.
[54] Tao H, Marelli B, Yang M, An B, Onses MS, Rogers JA, et al. Inkjet printing of regenerated silk fibroin: from printable forms to printable functions. Adv Mater 2015;27(29):4273–9.

[55] Rider PM, Brook IM, Smith PJ, Miller CA. Reactive inkjet printing of regenerated silk fibroin films for use as dental barrier membranes. Micromachines 2018;9(2):46.
[56] Gregory DA, Kumar P, Jimenez-Franco A, Zhang Y, Zhang Y, Ebbens SJ, et al. Reactive inkjet printing and propulsion analysis of silk-based self-propelled micro-stirrers. Jove-J Vis Exp 2019;146:e59030.
[57] Zhang Y, Gregory DA, Zhang Y, Smith PJ, Ebbens SJ, Zhao X. Reactive inkjet printing of functional silk stirrers for enhanced mixing and sensing. Small 2019;15(1):1804213.
[58] Liu Z, Zhou Z, Zhang S, Sun L, Shi Z, Mao Y, et al. "Print-to-pattern": silk-based water lithography. Small 2018;14(47):1802953.
[59] Huang JN, Xu ZJ, Qiu W, Chen F, Meng ZH, Hou C, et al. Stretchable and heat-resistant protein-based electronic skin for human thermoregulation. Adv Funct Mater 2020;30(13):1910547.
[60] Limem S, Calvert P, Kim HJ, Kaplan DL. Differentiation of bone marrow stem cells on inkjet printed silk lines. MRS Proc 2006;950.
[61] Suntivich R, Drachuk I, Calabrese R, Kaplan DL, Tsukruk VV. Inkjet printing of silk nest arrays for cell hosting. Biomacromolecules 2014;15(4):1428–35.
[62] Drachuk I, Suntivich R, Calabrese R, Harbaugh S, Kelley-Loughnane N, Kaplan DL, et al. Printed dual cell arrays for multiplexed sensing. ACS Biomater Sci Eng 2015;1(5):287–94.
[63] Compaan AM, Christensen K, Huang Y. Inkjet bioprinting of 3D silk fibroin cellular constructs using sacrificial alginate. ACS Biomater Sci Eng 2017;3(8):1519–26.
[64] Guo C, Li C, Vu HV, Hanna P, Lechtig A, Qiu Y, et al. Thermoplastic moulding of regenerated silk. Nat Mater 2020;19(1):102–8.
[65] Cesarano J, Segalman R, Calvert P. Robocasting provides mouldless fabrication from slurry deposition. Ceram Ind 1998;148(4):94–6.
[66] Cesarano J III, Calvert P, inventor. Corporation S, assignee. Freeforming objects with low-binder slurry. United States patent US 06027326A. 2000 Feb 22.
[67] Mooney M. Explicit formulas for slip and fluidity. J Rheol 1931;2(2):210–22.
[68] Christopher RH, Middleman S. Power–law flow through a packed tube. Ind Eng Chem Fundam 1965;4(4):422–6.
[69] Schaffner M, Faber JA, Pianegonda L, Rühs PA, Coulter F, Studart AR. 3D printing of robotic soft actuators with programmable bioinspired architectures. Nat Commun 2018;9(1):878.
[70] Murphy SV, Atala A. 3D bioprinting of tissues and organs. Nat Biotechnol 2014;32(8):773–85.
[71] Mu X, Gonzalez-Obeso C, Xia Z, Sahoo JK, Li G, Cebe P, et al. 3D printing of monolithic proteinaceous cantilevers using regenerated silk fibroin. Molecules 2022;27(7):2148.
[72] Kim E, Seok JM, Bae SB, Park SA, Park WH. Silk fibroin enhances cytocompatibilty and dimensional stability of alginate hydrogels for light-based three-dimensional bioprinting. Biomacromolecules 2021;22(5):1921–31.
[73] Kadumudi FB, Hasany M, Pierchala MK, Jahanshahi M, Taebnia N, Mehrali M, et al. The manufacture of unbreakable bionics via multifunctional and self-healing silk–graphene hydrogels. Adv Mater 2021;33(35):2100047.
[74] Huang L, Yuan W, Hong Y, Fan S, Yao X, Ren T, et al. 3D printed hydrogels with oxidized cellulose nanofibers and silk fibroin for the proliferation of lung epithelial stem cells. Cellulose 2021;28(1):241–57.
[75] Yang J, Deng C, Shafiq M, Li Z, Zhang Q, Du H, et al. Localized delivery of FTY-720 from 3D printed cell-laden gelatin/silk fibroin composite scaffolds for enhanced vascularized bone regeneration. Smart Mater Med 2022;3:217–29.
[76] Mu X, Wang Y, Guo C, Li Y, Ling S, Huang W, et al. 3D printing of silk protein structures by aqueous solvent-directed molecular assembly. Macromol Biosci 2020;20(1):1900191.
[77] Singh YP, Bandyopadhyay A, Mandal BB. 3D bioprinting using cross-linker-free silk–gelatin bioink for cartilage tissue engineering. ACS Appl Mater Interfaces 2019;11(37):33684–96.
[78] Das S, Pati F, Choi YJ, Rijal G, Shim JH, Kim SW, et al. Bioprintable, cell-laden silk fibroin–gelatin hydrogel supporting multilineage differentiation of stem cells for fabrication of three-dimensional tissue constructs. Acta Biomater 2015;11:233–46.
[79] Milazzo M, Fitzpatrick V, Owens CE, Carraretto IM, McKinley GH, Kaplan DL, et al. 3D printability of silk/hydroxyapatite composites for microprosthetic applications. ACS Biomater Sci Eng 2023;9(3):1285–95.
[80] Ghosh S, Parker ST, Wang X, Kaplan DL, Lewis JA. Direct-write assembly of microperiodic silk fibroin scaffolds for tissue engineering applications. Adv Funct Mater 2008;18(13):1883–9.
[81] Rodriguez MJ, Dixon TA, Cohen E, Huang W, Omenetto FG, Kaplan DL. 3D freeform printing of silk fibroin. Acta Biomater 2018;71:379–87.
[82] Ng P, Pinho AR, Gomes MC, Demidov Y, Krakor E, Grume D, et al. Fabrication of antibacterial, osteo-inductor 3D printed aerogel-based scaffolds by incorporation of drug laden hollow mesoporous silica microparticles into the self-assembled silk fibroin biopolymer. Macromol Biosci 2022;22(4):2100442.
[83] Gong D, Lin Q, Shao Z, Chen X, Yang Y. Preparing 3D-printable silk fibroin hydrogels with robustness by a two-step crosslinking method. RSC Adv 2020;10(45):27225–34.
[84] Heichel DL, Tumbic JA, Boch ME, Ma AW, Burke KA. Silk fibroin reactive inks for 3D printing crypt-like structures. Biomed Mater 2020;15(5):055037.
[85] Zhou M, Wu X, Luo J, Yang G, Lu Y, Lin S, et al. Copper peptide-incorporated 3D-printed silk-based scaffolds promote vascularized bone regeneration. Chem Eng J 2021;422:130147.
[86] Sharma A, Rawal P, Tripathi DM, Alodiya D, Sarin SK, Kaur S, et al. Upgrading hepatic differentiation and functions on 3D printed silk-decellularized liver hybrid scaffolds. ACS Biomater Sci Eng 2021;7(8):3861–73.
[87] Jiang S, Yu Z, Zhang L, Wang G, Dai X, Lian X, et al. Effects of different aperture-sized type I collagen/silk fibroin scaffolds on the proliferation and differentiation of human dental pulp cells. Regen Biomater 2021;8(4):rbab028.
[88] Li XH, Zhu X, Liu XY, Xu HH, Jiang W, Wang JJ, et al. The corticospinal tract structure of collagen/silk fibroin scaffold implants using 3D printing promotes functional recovery after complete spinal cord transection in rats. J Mater Sci: Mater Med 2021;32(4):31–2.
[89] Li H, Li N, Zhang H, Zhang Y, Suo H, Wang L, et al. Three-dimensional bioprinting of perfusable hierarchical microchannels with alginate and silk fibroin double cross-linked network. 3D Print Addit Manuf 2020;7:78–84.
[90] Zheng Z, Wu J, Liu M, Wang H, Li C, Rodriguez MJ, et al. 3D bioprinting of self-standing silk-based bioink. Adv Healthc Mater 2018;7(6):1701026.
[91] Fitzpatrick V, Martín-Moldes Z, Deck A, Torres-Sanchez R, Valat A, Cairns D, et al. Functionalized 3D-printed silk-hydroxyapatite scaffolds for enhanced bone regeneration with innervation and vascularization. Biomaterials 2021;276:120995.
[92] Li Q, Xu S, Feng Q, Dai Q, Yao L, Zhang Y, et al. 3D printed silk-gelatin hydrogel scaffold with different porous structure and cell seeding strategy for cartilage regeneration. Bioact Mater 2021;6(10):3396–410.
[93] Bhunia BK, Dey S, Bandyopadhyay A, Mandal BB. 3D printing of annulus fibrosus anatomical equivalents recapitulating angle-ply architecture for intervertebral disc replacement. Appl Mater Today 2021;23:101031.
[94] Karamat-Ullah N, Demidov Y, Schramm M, Grumme D, Auer J, Bohr C, et al. 3D printing of antibacterial, biocompatible, and biomimetic hybrid aerogel-based scaffolds with hierarchical porosities via integrating antibacterial peptide-modified silk fibroin with silica nanostructure. ACS Biomater Sci Eng 2021;7(9):4545–56.
[95] Dorishetty P, Balu R, Gelmi A, Mata JP, Dutta NK, Choudhury NR. 3D printable soy/silk hybrid hydrogels for tissue engineering applications. Biomacromolecules 2021;22(9):3668–78.
[96] Maleki H, Montes S, Hayati-Roodbari N, Putz F, Huesing N. Compressible, thermally insulating, and fire retardant aerogels through self-assembling silk fibroin biopolymers inside a silica structure—an approach towards 3D printing of aerogels. ACS Appl Mater Interfaces 2018;10(26):22718–30.
[97] Dorishetty P, Balu R, Athukoralalage SS, Greaves TL, Mata J, De Campo L, et al. Tunable biomimetic hydrogels from silk fibroin and nanocellulose. ACS Sustain Chem & Eng 2020;8(6):2375–89.
[98] Zhong N, Dong T, Chen Z, Guo Y, Shao Z, Zhao X. A novel 3D-printed silk fibroin-based scaffold facilitates tracheal epithelium proliferation *in vitro*. J Biomater Appl 2019;34(1):3–11.
[99] Bon SB, Chiesa I, Degli Esposti M, Morselli D, Fabbri P, De Maria C, et al. Carbon nanotubes/regenerated silk composite as a three-dimensional printable bio-adhesive ink with self-powering properties. ACS Appl Mater Interfaces 2021;13(18):21007–17.
[100] Patel DK, Dutta SD, Hexiu J, Ganguly K, Lim KT. 3D-printable chitosan/silk fibroin/cellulose nanoparticle scaffolds for bone regeneration via M2 macrophage polarization. Carbohydr Polym 2022;281:119077.
[101] Huang L, Du X, Fan S, Yang G, Shao H, Li D, et al. Bacterial cellulose nanofibers promote stress and fidelity of 3D-printed silk based hydrogel scaffold with hierarchical pores. Carbohydr Polym 2019;221:146–56.
[102] Huang T, Fan C, Zhu M, Zhu Y, Zhang W, Li L. 3D-printed scaffolds of biomineralized hydroxyapatite nanocomposite on silk fibroin for improving bone regeneration. Appl Surf Sci 2019;467–468:345–53.
[103] Wei L, Wu S, Kuss M, Jiang X, Sun R, Reid P, et al. 3D printing of silk fibroin-based hybrid scaffold treated with platelet rich plasma for bone tissue engineering. Bioact Mater 2019;4:256–60.
[104] Wang J, Goyanes A, Gaisford S, Basit AW. Stereolithographic (SLA) 3D printing of oral modified-release dosage forms. Int J Pharm 2016;503(1–2):207–12.
[105] Wadnap S, Krishnamoorthy S, Zhang Z, Xu C. Biofabrication of 3D cell-encapsulated tubular constructs using dynamic optical projection stereolithography. J Mater Sci: Mater Med 2019;30(3):36.
[106] Melchels FP, Feijen J, Grijpma DW. A review on stereolithography and its applications in biomedical engineering. Biomaterials 2010;31(24):6121–30.
[107] Murphy CA, Lim KS, Woodfield TB. Next evolution in organ–scale biofabrication: bioresin design for rapid high-resolution vat polymerization. Adv Mater 2022;34(20):2107759.
[108] Suri S, Han LH, Zhang W, Singh A, Chen S, Schmidt CE. Solid freeform fabrication of designer scaffolds of hyaluronic acid for nerve tissue engineering. Biomed Microdevices 2011;13(6):983–93.
[109] Yu C, Schimelman J, Wang PR, Miller KL, Ma XY, You ST, et al. Photopolymerizable biomaterials and light-based 3D printing strategies for biomedical applications. Chem Rev 2020;120(19):10695–743.
[110] Gastaldi M, Cardano F, Zanetti M, Viscardi G, Barolo C, Bordiga S, et al. Functional dyes in polymeric 3D printing: applications and perspectives. ACS Materials Lett 2021;3(1):1–17.
[111] Yu K, Zhang XJ, Sun Y, Gao Q, Fu JZ, Cai XJ, et al. Printability during projection-based 3D bioprinting. Bioact Mater 2022;11:254–67.
[112] Shin S, Kwak H, Hyun J. Melanin nanoparticle-incorporated silk fibroin hydrogels for the enhancement of printing resolution in 3D-projection stereolithography of poly(ethylene glycol)-tetraacrylate bio-ink. ACS Appl Mater Interfaces 2018;10(28):23573–82.

[113] Kim SH, Yeon YK, Lee JM, Chao JR, Lee YJ, Seo YB, et al. Precisely printable and biocompatible silk fibroin bioink for digital light processing 3D printing. Nat Commun 2018;9(1):2350.
[114] Ajiteru O, Sultan MT, Lee YJ, Seo YB, Hong H, Lee JS, et al. A 3D printable electroconductive biocomposite bioink based on silk fibroin-conjugated graphene oxide. Nano Lett 2020;20(9):6873–83.
[115] Ajiteru O, Choi KY, Lim TH, Kim DY, Hong H, Lee YJ, et al. A digital light processing 3D printed magnetic bioreactor system using silk magnetic bioink. Biofabrication 2021;13(3):034102.
[116] Egawa S, Kurita H, Kanno T, Narita F. Effect of silk fibroin concentration on the properties of polyethylene glycol dimethacrylates for digital light processing printing. Adv Eng Mater 2021;23(9):2100487.
[117] Mu X, Sahoo JK, Cebe P, Kaplan DL. Photo-crosslinked silk fibroin for 3D printing. Polymers 2020;12(12):2936.
[118] Shin D, Hyun J. Silk fibroin microneedles fabricated by digital light processing 3D printing. J Ind Eng Chem 2021;95:126–33.
[119] Xie M, Lian L, Mu X, Luo Z, Garciamendez-Mijares CE, Zhang Z, et al. Volumetric additive manufacturing of pristine silk-based (bio)inks. Nat Commun 2023;14(1):210.
[120] Lee H, Shin D, Shin S, Hyun J. Effect of gelatin on dimensional stability of silk fibroin hydrogel structures fabricated by digital light processing 3D printing. J Ind Eng Chem 2020;89:119–27.
[121] Na K, Shin S, Lee H, Shin D, Baek J, Kwak H, et al. Effect of solution viscosity on retardation of cell sedimentation in DLP 3D printing of gelatin methacrylate/silk fibroin bioink. J Ind Eng Chem 2018;61:340–7.
[122] Kwak H, Shin S, Lee H, Hyun J. Formation of a keratin layer with silk fibroin–polyethylene glycol composite hydrogel fabricated by digital light processing 3D printing. J Ind Eng Chem 2019;72:232–40.
[123] Hong H, Seo YB, Kim DY, Lee JS, Lee YJ, Lee H, et al. Digital light processing 3D printed silk fibroin hydrogel for cartilage tissue engineering. Biomaterials 2020;232:119679.
[124] Liang R, Shen X, Xie C, Gu Y, Li J, Wu H, et al. Silk gel recruits specific cell populations for scarless skin regeneration. Appl Mater Today 2021;23:101004.
[125] Kim SH, Seo YB, Yeon YK, Lee YJ, Park HS, Sultan MT, et al. 4D-bioprinted silk hydrogels for tissue engineering. Biomaterials 2020;260:120281.
[126] Kodama H. Automatic method for fabricating a three-dimensional plastic model with photo-hardening polymer. Rev Sci Instrum 1981;52(11):1770–3.
[127] Zhou LY, Fu J, He Y. A review of 3D printing technologies for soft polymer materials. Adv Funct Mater 2020;30(28):2000187.
[128] Tumbleston JR, Shirvanyants D, Ermoshkin N, Janusziewicz R, Johnson AR, Kelly D, et al. Continuous liquid interface production of 3D objects. Science 2015;347(6228):1349–52.
[129] Ligon SC, Liska R, Stampfl J, Gurr M, Mülhaupt R. Polymers for 3D printing and customized additive manufacturing. Chem Rev 2017;117(15):10212–90.
[130] Wu S, Serbin J, Gu M. Two-photon polymerisation for three-dimensional micro-fabrication. J Photochem Photobiol 2006;181(1):1–11.
[131] Valente F, Hepburn MS, Chen J, Aldana AA, Allardyce BJ, Shafei S, et al. Bioprinting silk fibroin using two-photon lithography enables control over the physico-chemical material properties and cellular response. Bioprinting 2022;25:e00183.
[132] Pawlicki M, Collins HA, Denning RG, Anderson HL. Two-photon absorption and the design of two-photon dyes. Angew Chem Int Edit 2009;48(18):3244–66.
[133] Cumpston BH, Ananthavel SP, Barlow S, Dyer DL, Ehrlich JE, Erskine LL, et al. Two-photon polymerization initiators for three-dimensional optical data storage and microfabrication. Nature 1999;398(6722):51–4.
[134] S. Tibbits, The emergence of "4D printing" [internet]. New York City: Technology, Entertainment, Design (TED) conference; 2013 Feb [cited 2022 Dec 10]. Available from: https://www.ted.com/talks/skylar_tibbits_the_emergence_of_4d_printing.
[135] Kuang X, Roach DJ, Wu J, Hamel CM, Ding Z, Wang T, et al. Advances in 4D printing: materials and applications. Adv Funct Mater 2019;29(2):1805290.
[136] El-Kady MF, Shao Y, Kaner RB. Graphene for batteries, supercapacitors and beyond. Nat Rev Mater 2016;1(7):16033.
[137] Lendlein A, Langer R. Biodegradable, elastic shape-memory polymers for potential biomedical applications. Science 2002;296(5573):1673–6.
[138] De Maria C, Chiesa I, Morselli D, Ceccarini MR, Bittolo Bon S, Degli Esposti M, et al. Biomimetic tendrils by four dimensional printing bimorph springs with torsion and contraction properties based on bio-compatible graphene/silk fibroin and poly (3-hydroxybutyrate-co-3-hydroxyvalerate). Adv Funct Mater 2021;31(52):2105665.
[139] Zheng H, Zuo B. Functional silk fibroin hydrogels: preparation, properties and applications. J Mater Chem B Mater Biol Med 2021;9(5):1238–58.
[140] Huang X, Zhang M, Ming J, Ning X, Bai S. High-strength and high-toughness silk fibroin hydrogels: a strategy using dynamic host-guest interactions. ACS Appl Bio Mater 2020;3(10):7103–12.
[141] Liu H, Sun Z, Guo C. Chemical modification of silk proteins: current status and future prospects. Adv Fiber Mater 2022;4(4):705–19.
[142] Murphy AR, Kaplan DL. Biomedical applications of chemically-modified silk fibroin. J Mater Chem 2009;19(36):6443–50.
[143] Heichel DL, Burke KA. Dual-mode cross-linking enhances adhesion of silk fibroin hydrogels to intestinal tissue. ACS Biomater Sci Eng 2019;5(7):3246–59.